Fall 2009

Duty Cycle Maintenance in an Artificial Neuron

William Halbert Barnett
Georgia State University

DUTY CYCLE MAINTENANCE IN AN ARTIFICIAL NEURON

by

WILLIAM HALBERT BARNETT

Under the Direction of Dr. Gennady S. Cymbalyuk

ABSTRACT

Neuroprosthetics is at the intersection of neuroscience, biomedical engineering, and physics. A biocompatible neuroprosthesis contains artificial neurons exhibiting biophysically plausible dynamics. Hybrid systems analysis could be used to prototype such artificial neurons. Biohybrid systems are composed of artificial and living neurons coupled via real-time computing and dynamic clamp. Model neurons must be thoroughly tested before coupled with a living cell. We use bifurcation theory to identify hazardous regimes of activity that may compromise biocompatibility and to identify control strategies for regimes of activity desirable for functional behavior. We construct real-time artificial neurons for the analysis of hybrid systems and demonstrate a mechanism through which an artificial neuron could maintain duty cycle independent of variations in period.

INDEX WORDS: Hybrid systems, Real time systems, Hodgkin huxley, Neuronal dynamics, Electrophysiology, Dynamic clamp, Medicinal leech, Central pattern generator, Half center oscillator, Heartbeat, Bifurcation theory,

DUTY CYCLE MAINTENANCE IN AN ARTIFICIAL NEURON

by

WILLIAM HALBERT BARNETT

A Thesis Submitted in Partial Fulfillment of the Requirements for the Degree of

Master of Science

in the College of Arts and Sciences

Georgia State University

2009

DUTY CYCLE MAINTENANCE IN AN ARTIFICIAL NEURON

by

WILLIAM HALBERT BARNETT

Committee Chair: Gennady Cymbalyuk

Committee: Vadym Apalkov

Mukesh Dhamala

Andrey Shilnikov

Electronic Version Approved:

Office of Graduate Studies

College of Arts and Sciences

Georgia State University

DEDICATION

I would like to dedicate this thesis to Bill Barnett.

ACKNOWLEDGEMENTS

I would like to thank Martin Anquez and Dr. Gennady Cymbalyuk.

I am grateful for support from NSF grant PHY-0750456 to GC, and I here show my appreciation for an equipment grant (Spring 2009) and two travel awards (Spring 2008 and Spring 2009) from the Center for Neuromics.

TABLE OF CONTENTS

LIST OF FIGURES

1. INTRODUCTION

Dysfunction in the operation of the nervous system can elicit behavioral disorder and disability that disrupts mobility and livelihood. Neuroprosthetics is a new, frontier discipline at the intersection of neuroscience and biomedical engineering which has proven itself efficient in returning hearing, sight, and mobility to people challenged by disabilities. In order to achieve a biocompatible neuroprosthesis, the artificial neurons must exhibit biophysically plausible dynamics. Hybrid systems analysis could be used to prototype such artificial neurons. Biohybrid systems are composed of artificial and living neurons coupled via real-time computing and dynamic clamp. Model neurons must be thoroughly tested before coupled with a living cell. We use bifurcation theory to identify hazardous regimes of activity that may compromise biocompatibility and to identify control strategies for regimes of activity desirable for functional behavior. We construct real-time artificial neurons for the analysis of hybrid systems and demonstrate a mechanism through which an artificial neuron could maintain duty cycle independent of variations in period.

One of its key goals is the design of neuroprostheses: implantable artificial devices restoring the functional dynamics of the corrupted neuronal circuit. There is a strong demand for a variety of tools for design and prototyping so that neuroprostheses can be manufactured at the industrial scale necessary for practical medical applications. They will be developed using the modern technology of computer-brain interface based on real time systems, e.g. dynamic clamp and hybrid systems analysis.

Hybrid systems combine the parameter controllability of mathematical modeling with the physical realism of electrophysiological experiments. This approach allows biomedical engineers to assimilate electrophysiological techniques into the process of

development. As such, the implementation of hybrid systems is facilitated by developments in dynamic clamp and real-time computing. These hybrid systems require software operating in real time on a timescale fast compared to the time constants of ionic currents involved. Designated real time controllers are necessary to fulfill these real time requirements. A real time controller is a computer that performs computational tasks on a strict schedule. Using such a system to control a dynamic clamp enables real time interaction between simulated and biological cells. Dynamic clamp has been used to implement artificial ionic currents in and synapses between living cells (Sharp et al., 1993; Dorval et al., 2001; Butera et al., 2001; Pinto et al., 2001). In hybrid systems, dynamic clamp provides the interface between the simulated and living neurons (Manor & Nadim, 2001).

The prototyping of a control system proceeds in several stages. First, we design a mathematical model which incorporates everything we know about the dynamics of the functional unit, the neuronal sub-circuit, or the neuron. Then we investigate the dynamics of the model. Different regimes of activity span a high dimensional parameter space in a typical Hodgkin-Huxley style neuronal model. We establish a subset of this space for which the resultant model activities share important traits with activity observed in the healthy neuronal system. Among the important characteristics are spike frequency, burst frequency, burst duration, coexistence of oscillations and silence, and other properties of excitability. Detailed analysis of these parameters' space allows a researcher to select optimal parameter values for the task at hand. This process is repeated for the intended synaptic target of the artificial neuron. Next we can create a hybrid system and test the prototype for its functionality in reality. After any drawbacks and catastrophes of the

hybrid have been studied and classified, a new generation of the prototype is to be designed and tested.

Hybrid systems analysis is a powerful technique that has proven itself in neuroscience. It is useful as a prototyping tool for biomedical engineers. Previously, the technology has been used to identify the role of individual currents in specific cellular mechanisms(Sorensen et al., 2004; Olypher et al., 2006). The intent of prototyping may be to establish a certain stable regime of circuit activity, but it is hybrid systems analysis that we use to reveal the effect of explicitly defined ionic currents of the artificial cell on the activity of a neural circuit. By replacing a component of a living circuit with a computational cell, we may gain knowledge of its role in the circuit by manipulating parameters of artificial ionic currents. With prototyping, we seek to take the knowledge of the role of individual ionic currents and move an unhealthy circuit from a pathological regime to a healthy regime. We present a set of experiments performed on the leech heart interneuron as an example of prototyping and hybrid systems analysis. The first study utilizes a VLSI silicon artificial neuron in which I_h is tuned to examine its interaction with the synaptic current (Sorensen et al., 2004). The second study uses computational neurons built with the library we present in 8.2.3 to tune the slow Ca^{2+} current to show its role in supporting bursting activity (Olypher et al., 2006).

Model Leech Heart Interneuron Synapse

The canonical model of the leech heart interneuron is composed of eight voltage gated currents and a leak current (Hill et al., 2001). The eight voltage gated currents are composed of thirteen gating variables. The mathematical model is composed of fourteen equations: one for the membrane potential and one each for the gating variables. The

hybrid system contains a synapse from the artificial cell onto the living cell and a synapse from the living cell onto the artificial cell. The synaptic current has a spike-mediated component and a slower modulating component, so the system requires an additional six differential equations:

$$I_{Syn} = \bar{g}_{Syn} Y_{post} M_{post} \left[V_{post} - E_{post}\right]$$

$$\frac{dX_{post}}{dt} = \frac{\left[X_{\infty}(V_{pre}) - X_{post}\right]}{0.002}$$

$$\frac{dY_{post}}{dt} = \frac{\left[X_{post} - Y_{post}\right]}{0.011}$$

$$\frac{dM_{post}}{dt} = \frac{\left[M_{\infty}(V_{pre}) - M_{post}\right]}{0.2},$$

$$X_{\infty}(V_{pre}) = \frac{1}{1+\exp\left(-1000\left[V_{pre}+0.01\right]\right)};\ M_{\infty}(V_{pre}) = 0.1 + \frac{0.9}{1+\exp\left(-1000\left[V_{pre}+0.04\right]\right)}.$$

The membrane potential of the living cell is recorded and passed into the model system where it is used to evaluate the synaptic current onto the artificial cell. The membrane potential of the artificial cell is used to evaluate the synaptic current onto the living cell, which is passed out of the system to be injected by an amplifier into the live cell. We are able integrate each of these operations with Euler's method for numerical integration at 10 to 20 kHz on the DS1103 PPC board. At these frequencies, the artificial system performs sufficiently fast to produce biophysically plausible trajectories.

Hybrid Systems Analysis

Observations with sharp intracellular electrodes have shown that the HNs spike tonically when pharmacologically isolated from the cholinergic synapse with bicuculline methiodide (Schmidt & Calabrese, 1992). However, recordings with extracellular electrodes under the same pharmacological conditions show that HNs burst endogenously (Cymbalyuk et al., 2002). The model shows evidence that a nonspecific leak current,

introduced by piercing the cell with a sharp electrode, is responsible for the onset of tonic spiking. In order to implement a hybrid system, a sharp electrode is used to inject an artificial current into the living cell. Even though the HN is an endogenously bursting cell, dynamic clamp experiments are performed while the cell is in a tonic spiking mode. Nevertheless, a mutually inhibitory artificial synapse by and onto a bursting model cell is sufficient to reinitiate antiphase bursting in the living HN (Sorensen et al., 2004; Olypher et al., 2006). We tune the hybrid system by manipulating parameters of the artificial cell to identify the mechanisms supporting the half center oscillator.

In order to establish a biophysically plausible hybrid half center oscillator, a certain amount of tuning is necessary. Key parameters for temporal regulation can be identified in an analysis of the parameter space ahead of time (Hill et al., 2001; Cymbalyuk et al., 2002), such that the artificial cell can be adapted to its intended synaptic target quickly at run time. The uncoupled artificial cell must exhibit slow oscillations of roughly the same duration as its living synaptic target; Olypher et al., (2006) adapted the leak current to this end. In order to appropriately model the activation of the synaptic current, the temporal characteristics of individual action potentials must be conserved between the model and the living cell. Due to VLSI transistor mismatch, Sorensen et al., (2004) were forced to adjust spiking characteristics by changing parameters of fast variables.

The heartbeat of the leech is controlled by a central pattern generator (CPG). The kernel of this CPG consists of pairs of bursting HN cells, which form half center oscillators. Each HN cell possesses an inhibitory and spike-mediated cholinergic synaptic current (Schmidt & Calabrese, 1992). As one cell bursts, the synaptic current onto the second cell suppresses the activity of the second cell, forming the quiescent phase between bursts. The

prolonged hyperpolarization during the interburst interval activates I_h and removes the inactivation of I_{CaS}, the slow Ca^{2+} current (Hill et al., 2001). In this way, I_{Syn} and I_h on the inhibited neuron control the interburst interval of that neuron (Sorensen et al., 2004). I_{Syn} causes the hyperpolarization of quiescence and I_h produces the rebound to a depolarized state. Upon depolarization, the conductance of I_{CaS} becomes very large and slowly dwindles as the current is inactivated (Olypher et al., 2006). This long lasting inward current supports the plateau depolarization of the burst and regulates the spike frequency.

The experiments that ascertain the role of I_h and I_{CaS} encapsulate the core essence of prototyping. Sorensen et al. (2004) show that by decreasing g_h in the artificial cell, the interburst interval of the artificial cell increases. Because the resistance of I_h to synaptic inhibition has decreased, the artificial cell takes longer to escape the quiescent phase. Consequently, the burst phase of the HN increases in duration due to the delayed inhibiting input. When g_h is increased in the artificial cell, its resistance to inhibition increases, and the interburst interval of the artificial cell decreases in duration. Meanwhile, the burst duration of HN decreases because of the earlier onset of inhibition from the artificial cell. Olypher et al. (2006) describe the role of I_{CaS} with a similar set of experiments. By decreasing the time constant of inactivation of I_{CaS}, $\tau_{h,CaS}$, the conductance of I_{CaS} falls is inactivated at a greater rate in response to the depolarization of the burst, so the bursts are shorter, and the interburst interval of the presynaptic HN is shortened by the reduced synaptic inhibition. An increase in $\tau_{h,CaS}$ in the artificial cell allows I_{CaS} to stay active for a longer period, and the burst duration is greater. The prolonged burst of the artificial cells leads to a prolonged synaptic current on the HN. The quiescent phase of the HN increases as well.

Prototype Reduced Heart Interneuron

We explore the role of a hyperpolarization activated current and a potassium current in the periodicity of a Hodgkin-Huxley style neuronal model, by manipulating the half activation voltage of each. The half activation of K^+ currents has been shown to be regulated by dopamine and serotonin in the pyloric network (Peck et al., 2001). The half activation of I_h has been modulated by noradrenalin and serotonin in guinea-pigs and cats, by Ca^{2+} in ferrets, and by cAMP in ferrets and rats (McCormick & Pape, 1990; Luthi & McCormick, 1998; Luthi & McCormick, 1999).

Central pattern generators are neuronal networks that control different types of rhythmic movement. Many of these neuronal circuits maintain phase as the period of activity changes. Some examples are the network controlling swim behavior in the lamprey (Wallen & Williams, 1983), the leech heart beat (Wenning et al., 2003; Norris et al., 2006; Norris et al., 2007), the swim motor pattern in the leech (Friesen & Pearce, 1993), and the lobster pyloric rhythm (Hooper, 1997). Experimental and theoretical studies show that phase maintenance may be mediated by synaptic currents (Eisen & Marder, 1984; Nadim et al., 2003), and modeling evidence suggests that slow gating variables may also support phase maintenance (Hooper et al., 2009).

In the network controlling the heart beat of the leech, duty cycle is maintained independent of period as well as phase (Norris et al., 2006; Norris et al., 2007). By studying the role of these two currents in the maintenance of duty cycle, we show the role of neuromodulation in maintenance of function critical cell characteristics. We approach the problem of temporal coordination in central pattern generators by proposing a mechanism through which ionic currents intrinsic to a cell could maintain duty cycle. Ultimately, we

create a prototype artificial neuron with the ability to adapt an aspect of its intrinsic activity in response to external stimuli.

Our model is a variant on previously published pharmacologically reduced models of the leech heart interneuron (Cymbalyuk & Calabrese, 2001; Shilnikov & Cymbalyuk, 2005). It is convenient to use this reduced model because the inducing pharmacological scenario (described below) allows the HN cell to continue to burst after being pierced with a sharp electrode. In this way, each of our modeling results could be verified experimentally by implementation of a hybrid system with dynamic clamp in a manner similar to Sorensen et al. (2004) and Olypher. et al. (2006).

In this manuscript, we describe an easy to learn and use technique with which to perform hybrid systems analysis. We include a library of functions that are sufficient to implement a typical dynamic clamp and to construct any Hodgkin-Huxley style model of a neuron. Then, we provide an example of a real-time implementation of the Hodgkin Huxley model of the squid giant axon. By manipulating the voltage dependency of activation in each of the slow currents in the reduced HN, we show the role of each in bursting activity. We describe general trends in periodicity as these parameters are varied. We identify congruent regimes of activity in which the duty cycle of bursting activity is preserved.

2. APPLICATION OF TECHNOLOGY FOR HYBRID SYSTEMS

The automotive, aerospace, and robotics industries rely on extensive prototyping of the control systems by using technologies of the real-time systems. The same technologies can be used for the development and testing of the neuroprostheses by using hybrid systems analysis. A number of dynamic clamp solutions exist that satisfy the requirements for real-time computation. Real-Time Linux Dynamic Clamp (Dorval et al., 2001) and now Real-Time eXperiment Interface (RTXI; www.rtxi.org) are open source platforms based on the real-time kernel extension for the Linux operating system. National Instruments (Austin, TX) produces several lines of real-time PXI data acquisition boards in addition to the LabVIEW software suite which has been utilized for dynamic clamp (Kullmann et al., 2004). Milescu et al. (2008) have created a dynamic clamp extension for the QuB program (www.qub.buffalo.edu).

Hybrid systems need well defined control systems and a robust platform in order to operate effectively in real-time. Our models are built in Matlab & Simulink which is a programming environment for technical computing (The MathWorks, Inc., Natick, MA). Simulink has a graphically represented language with extensive libraries of functions for common mathematical and analytical tasks. Certain of these libraries, such as Real-Time Workshop, are dedicated to real-time and hardware targeted computing. We use dSPACE real-time boards: the DS1104 R&D and the DS1103 PPC. dSPACE, Inc. (Paderborn, Germany) produces and distributes a series of control system oriented real-time boards. A software package is bundled together with the dSPACE boards. It includes Real-Time Interface (RTI) and ControlDesk. RTI automatically utilizes block diagrams developed in Simulink into real-time code for dSPACE hardware. ControlDesk permits the building of a

graphical user interface with elaborate instrument panels that can be connected with corresponding model variables for interactive control of real-time application. dSPACE also provides a number of Simulink libraries for the design of control systems intended specifically for dSPACE hardware.

Our Simulink library is easy to use. Matlab & Simulink and the dSPACE hardware are over-the-counter and compatible with modern desktop computers. Additionally, LabVIEW provides a number of toolkits that allow Simulink models to be configured onto a number of National Instruments hardware targets. Our readymade templates for Hodgkin-Huxley type model components can be configured for a specific biological system and directly executed in real-time.

dSpace Boards

The dSpace DS1104 R&D and DS1103 PPC controller boards are extensively used in the automotive, aeronautical, and robotics industries to prototype control systems. These controllers can be installed in most modern desktop computers. The DS 1104 runs a Power PC 603e microprocessor at 250 MHz with 32 MB of SDRAM and 8 MB of flash memory. A 100-pin serial input/ output ribbon connects the board to the CP1104 data acquisition board. The CP1104 has 16 BNC ports. The input voltage range is ±10 V on eight analogue to digital conversion BNC ports. The first four ports are multiplexed over one channel with 16 bits of resolution. Each of the four remaining ports has a dedicated channel with 12 bits of resolution. The eight output ports each have a range of ±10 V with 16 bits of resolution. Each has a dedicated digital to analogue conversion channel.

The DS1103 is a full sized ISA card. Alternatively, it can be housed in an external box with a PCI card adapter for the host PC. This larger board is equipped with a Power PC

750GX microprocessor running at 1 GHz with 32 MB local and 96 MB global SDRAM. Data acquisition is performed on the CP 1103 board which links to the DS1103 via 3 parallel 100 pin serial ribbons. Thirty-two BNC ports are available over the range of ±10 V with 16 bits of resolution. Sixteen of the ports are analogue to digital input ports multiplexed over 4 channels. The eight digital to analogue output ports each has a dedicated channel.

While the dSpace boards are primarily used to design and test airplane and car control systems, they are efficient controllers for prototyping hybrid systems. Hardware specifications allow a board to simulate model neurons with the speed and fidelity necessary for electrophysiological protocols. When paired with standard laboratory equipment such as the AxoClamp-2B (Axon Instruments, CA), a Simulink model can efficiently run dynamic clamp in real time on the DS1104 or DS1103.

Introduction to Programming in Simulink

Our dynamic clamp is implemented as a Simulink block diagram. We provide a library of functions which can be used to tailor it to specific needs. We have included a model of an oscillatory leech heart interneuron as well as basic functions for the construction of Hodgkin-Huxley type neuronal models and functions to implement all standard dynamic clamp features.

Simulink is a graphical programming language for designing control systems in the MatLab programming environment. Operations and functions are represented by individual blocks or groups of blocks, and the flow of the program is made explicit by arrowed lines connecting each block. Blocks have input ports, where arguments and parameters are passed into the block, and output ports where the block returns the results of the operations or functions that it represents. Depending on the type of block, double

clicking on a block allows the user to access its properties and options, embedded code, or the embedded subsystem of blocks. Simulink comes with 15 basic libraries of blocks in addition to several specialized libraries. The basic libraries contain blocks for math functions and signal processing, while the specialized libraries are targeted for more specific applications such as real-time control.

A small set of basic blocks is sufficient to create a neuronal model based on the Hodgkin-Huxley formalism (Figure1A). Each of these blocks has a number of modes and functions that can be changed by the developer. The number of input ports and output ports depends on the block configuration. The Constant block supplies an unchanging signal of amplitude specified by the user. The Gain block multiplies its input signal by a factor specified by the user. This can be used in place of the Multiplication/ Division block. The Multiplication/ Division block is versatile; the number and type of inputs can be tailored to the task at hand. It accepts scalar, vector, or matrix input. It is also possible to specify element-wise or matrix operations. Setting this block with a single port that performs division is equivalent to obtaining the reciprocal for scalar inputs and performing matrix inversion on matrix inputs. Similarly, the Add/ Subtract block has variable input ports and acts on both scalar and vector inputs. The Integration block performs numerical integration. There both fixed step and variable step solvers available to the developer. The initial conditions for integration can be defined as a parameter internal to the box, or it can be passed in as an argument. The Math Function block can be set to compute exponents, natural logarithms, powers of ten, logarithms of base ten, complex amplitude, squares,

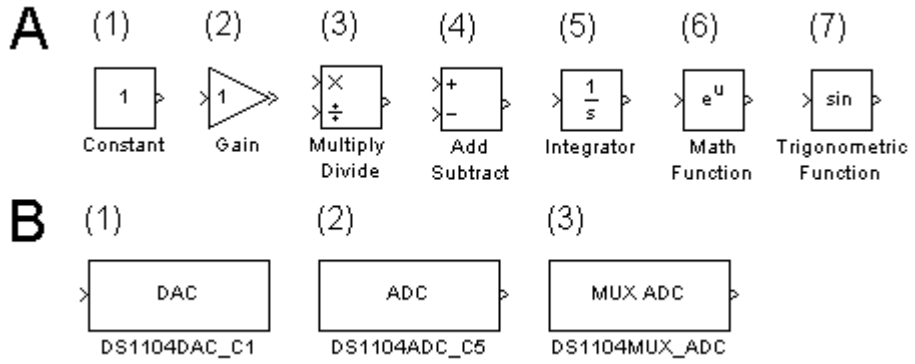

Figure 1. **Basic blocks.** In Simulink, programs are represented as diagrams built out of elemental blocks. Each block represents an individual operation. (A) A small number of blocks representing basic mathematical functions are sufficient to create Hodgkin-Huxley style neuronal models. (B) dSpace blocks provide Simulink models with a means to interact with real world systems. (B 1,2) Channels with dedicated BNC ports can be accessed with individual blocks. The number at the end of the block name corresponds to the channel number of the port on the CP1104 board. (B3) The 16 bit analogue to digital conversion channels are multiplexed. Internal block setting allow the developer to specify to which ports the block is connected.

square roots, powers defined by input, complex conjugation, reciprocals, hypotenuses, remainders, modulus, transposes and complex conjugate transposes. The Trigonometric Function block can perform functions including sine, cosine, tangent, arcsine, arccosine, arctangent, hyperbolic sine, hyperbolic cosine, hyperbolic tangent, and hyperbolic arctangent.

These Simulink blocks are sufficient to create sophisticated neuronal models, but do not provide us with a tool to interact with external systems. In order for a model to be useful for hybrid systems, a control signal from the system must be passed to an amplifier and into a cell as current, and the amplifier must feed the membrane potential of the cell back to the model. We move the simulation of the system off of the desktop computer and onto a peripheral dSPACE board specialized for control systems. dSPACE has provided a set of Simulink blocks for writing data to and reading data from devices such as an amplifier.

By passing the desired control signal from a model into a dSPACE block, the signal is routed out through the data acquisition board to the amplifier. Similarly, a dSPACE block acts as a source in a Simulink block diagram by routing the membrane potential of the cell back onto the control board. Blocks compatible with the DS1104 board are located in the DS1104 MASTER PPC library which is located in the dSPACE RTI1104 PPC directory in the Simulink library browser. dSPACE blocks allow the control system to interact with other devices via specific ports on the CP1104 (Figure 1B). The DS1104ADC_C5 block reads input from the board with 12-bit resolution. The C5 suffix indicates that the block corresponds to port five, but the block is applicable for ADC ports five through eight. The DS1104DAC_C1 block writes to the digital to analogue port on with 16-bit resolution and is applicable for all eight digital to analogue ports. For the DS1104DAC and DS1104ADC blocks, the user can specify the channel to which it is associated by changing the number in the suffix to the desired port number provided that it is within the applicable range. Finally, the DS1104MUX_ADC block reads from analogue to digital ports one through four at 16-bits. In order to specify which port or ports, it is necessary to change the settings of the block.

Library for Dynamic Clamp

The dynamic clamp is a tool used to perform electrophysiological experiments by injecting current of with particular dynamical characteristics into a living cell. In this manner, an artificial current with the characteristics defined by the researcher can be introduced in addition to the existing set of ionic currents endogenous to the membrane. Alternatively, the dynamic clamp can be used to substitute an artificial current with desirable characteristics for an endogenous ionic current. A hybrid system uses the

dynamic clamp as the link between the computational and living aspects of the system in order to realize real time control of the temporal characteristics of neuronal dynamics.

Lets consider the hyperpolarization activated current (I_h) identified and measured (Angstadt & Calabrese, 1989) in the heart interneuron (HN) of the medicinal leech and then implemented in the canonical model of HN (Hill et al., 2001). The equations for the current and its activation are

$$m_{h\infty}(V) = \frac{1}{1+2\exp(180[V+0.047])+\exp(500[V+0.047])}, \quad (1)$$

$$\tau(V) = 0.7 + \frac{1.7}{1+\exp(-100[V+0.073])}, \quad (2)$$

$$\frac{dm_h}{dt} = \frac{m_{h\infty}(V)-m_h}{\tau(V)},$$

and

$$I_h = \overline{g_h} m_h^2 [V - E_h],$$

such that $\overline{g_h}$ is the maximal conductance, E_h is the reversal potential, and m_h is the activation variable. The functions $m_{h\infty}(V)$ and $\tau(V)$ are the steady state and time constant of activation. These types of models lend themselves to hierarchical organization. At the highest level, the model, environmental parameters and dSPACE links the data acquisition board are assigned. Descending into the model reveals a menagerie of blocks and subsystems.

A block diagram built to perform a specific task can be condensed into a single block so that complicated systems can be organized into a set of subsystems. A subsystem is a block diagram that is represented by a single block. Subsystems make it easy to conceptualize and organize the flow of operations in a block diagram by establishing a tree-like hierarchy to functional model components. Mundane details of computation can be

sequestered to lower hierarchical levels while control parameters can be readily available for manipulation closer to the root of the model.

At the lowest organizational level, system functions are evaluated. The operations performed at this level are primarily the calculations of steady state membrane potentials and gating variable time constants. The steady state membrane potential of I_h (1) is a Boltzmann function (represented by $f(b, V)$ in Figure 2A). The corresponding block diagram is inserted into the subsystem block hnInfh. The parameter b is an argument of the function and an input port of the block. It will be assigned by a Constant block at a higher organizational level. Other parameters of the function, such as the Gain blocks set at 180 and 500, can still be accessed from ControlDesk in real-time, but are left at this lower organizational level because there is no anticipation of accessing them. The steady state membrane potential for the activation of I_h is a unique function. The function for the voltage dependent time constant of activation, however, is used again and again in our model. From current to current, these functions are represented by the similar equations differing only in parameter values. Rather than build a dozen unique diagrams for time constant functions, a small set of equations can be reused to define many gating variables. A common equation for voltage dependent time constant (2) is also a Boltzmann function and contained in the subsystem block hnTau (represented by $f(a, b, c, d, V)$ in Figure 2B). In this case, each of the parameters is assigned at a higher organizational level so that the same block can be used in more than one gating variable.

The equation for the derivative of the activation of I_h is $\frac{dm_h}{dt}$ (Figure 3A). The Simulink subsystem block for this equation is mh with one input port, V, for the membrane potential and one output port, mh, for the value of the gating variable. Inside the

$$f(b,V) = \frac{1}{1 + 2 \cdot \exp(180 \cdot (b+V)) + \exp(500 \cdot (b+V))}$$

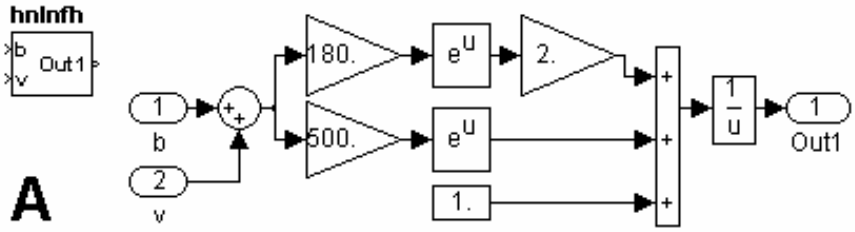

$$f(a,b,c,d,V) = c + \frac{d}{1 + \exp(a \cdot (b+V))}$$

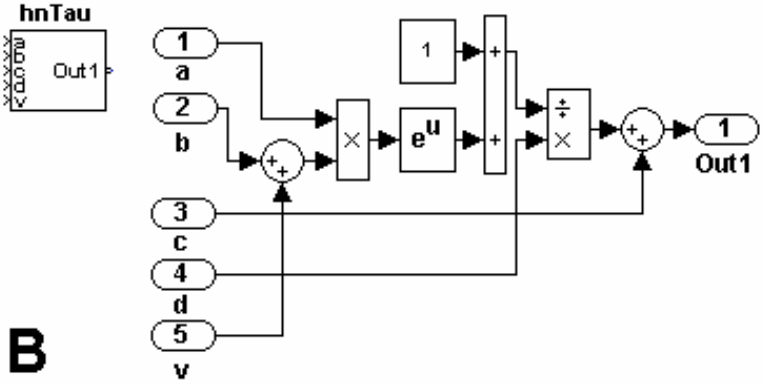

Figure 2. **Elemental Functions.** (A) The function $f(b,V)$ denotes the steady state membrane potential of I_h. The block diagram equivalent to $f(b,V)$ is embedded in the subsystem block *hnInfh*. In this case, a single parameter is defined at a higher organizational level. (B) The voltage dependent time constant of activation of I_h can be written as $f(a,b,c,d,V)$, and its block diagram is embedded in the subsystem block *hnTau*. This function is not unique to I_h. By defining many parameters at a higher organizational level, this block can be used for different time constants in other subsystems of the same model.

subsystem, the dynamics of the gating variable are defined by the steady state activation block hnInfh and the time constant block hnTau. At this hierarchical level, the parameters left undefined inside these blocks are passed in as arguments along with the membrane potential. It becomes important, when working in ControlDesk, to give these Constant blocks names that explicitly identify not only the parameter that each represents, but also

the specific current, variable, and function with which each is associated so that they may be differentiated from similar blocks in other subsystems.

Each ionic current is the product of its gating variable subsystems, maximum conductance, and driving force. Parameters for the maximal conductance and reversal potential are arguments to be passed into the system. Each ionic current subsystem has input ports for the membrane potential, the maximal conductance, and the reversal potential and output ports for the current and each of the intrinsic gating variables (Figure 3B). The neuronal model integrates the negative sum of the ionic currents in order to produce a value for membrane potential. This membrane potential is then passed into the ionic current systems to produce values for gating variables, driving forces, and ultimately a new value for each ionic current. This system itself is condensed into the HN neuron subsystem (Figure 4).

The mutually inhibitory HNs form a robust half center oscillator. Our model utilizes a fast spike mediated synapse as the agent of this inhibition (Cymalyuk et al., 2002; Hill et al., 2001). The activation and modulation of I_{Syn} are dynamical variables dependent on the presynaptic membrane potential. The driving force of the current, however, is a function of postsynaptic membrane potential. Spikes on the presynaptic cell lead to an increase in the conductance of the current, and the membrane potential of the postsynaptic cell determines how the cell will respond to the new current. The synaptic current on the postsynaptic cell is summed and integrated along with the intrinsic ionic currents of the membrane to produce a new value for the membrane potential. This new membrane potential is fed back into the intrinsic ionic current subsystems but is also passed out of the cell to determine the activation of the synapse onto the other cell. The neuronal subsystem

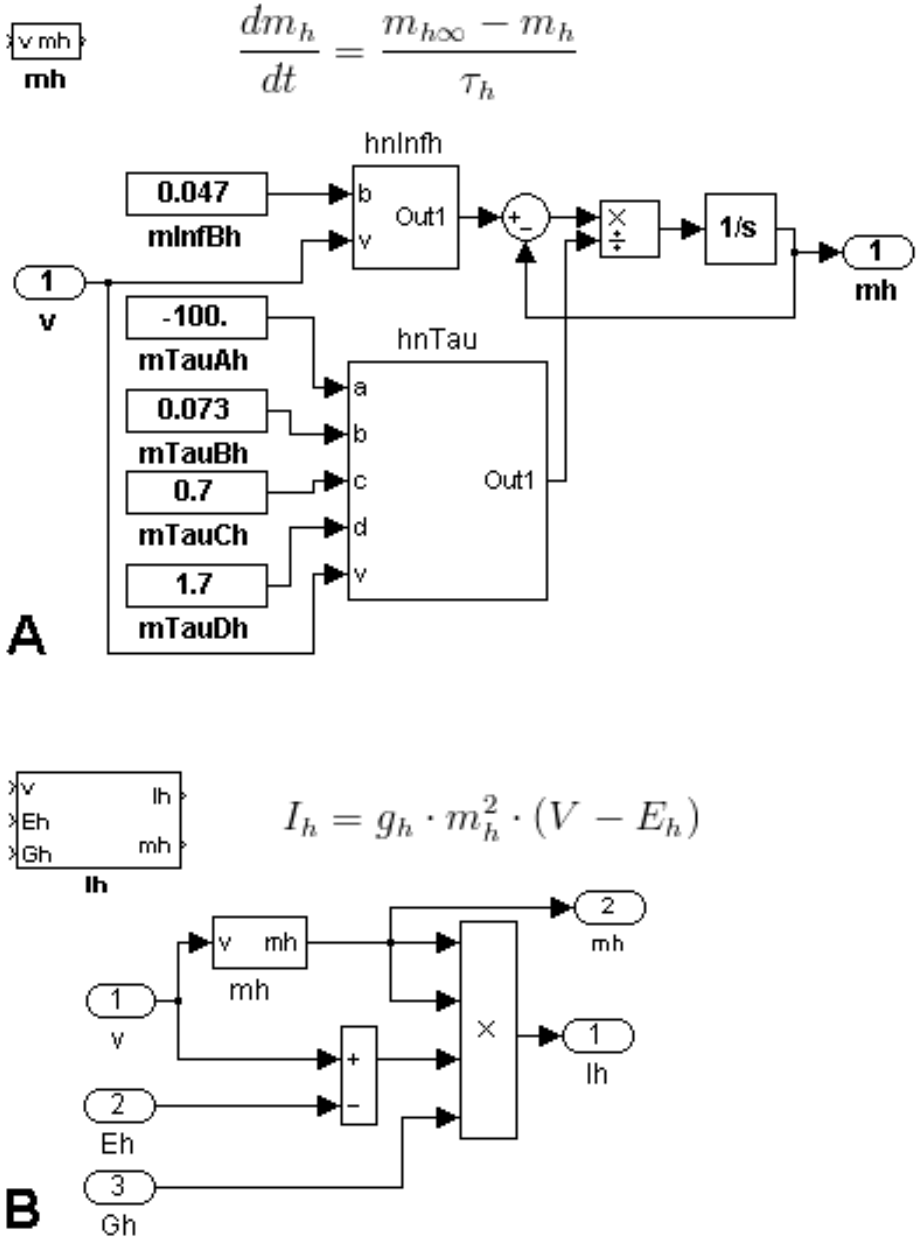

Figure 3. **Higher Level Equations.** (A) The activation variable for I_h is represented by the equation for $\frac{dm_h}{dt}$ and can be put together using preexisting functions for steady state of activation and time constant of activation (see Figure 5). At this hierarchical level, constants left undeclared in constituent functions are assigned and passed into the appropriate input ports. (B) The current subsystem, *Ih*, has two outputs: values for m_h and I_h. Functionally, the block is meant to evaluate the current, but it is convenient to pass out the activation variable as well, so that its dynamics can be recorded for further analysis.

HNwFastSyn implements the synaptic current by including the ISynS ionic current block and an additional input port for the presynaptic membrane potential.

A hybrid system has a living component as well as a computational component. An electrode placed inside of a neuron can read the membrane potential or inject current. Each of these processes is mediated by an amplifier and a data acquisition board, but these signals may be ultimately routed to a desktop computer. A procedure running in real-time allows a researcher to analyze captured data and directly control the dynamics of an injected current on the fly. By implementing our neuronal model in such a procedure, the model may interact with a living cell. The membrane potential of the living cell is read of the electrode and passed to the model running in real-time. This data feed is utilized to produce a synaptic response on the model neuron, and the response of the model cell is used to calculate a synaptic current which is then injected back into the living cell. The subsystem block MathAndLive demonstrates an implementation of just such a procedure on the DS1104 controller.

By connecting the voltage out and injected current command ports on an amplifier to the ADC and DAC ports on the CP1104 data acquisition board, the dSPACE ADC and DAC Simulink blocks provide a neuronal model direct access to its living counterpart. The membrane potential of the living cell is passed from the ADC block to the model cell where the live-to-math synapse is calculated. This current is summed with the intrinsic currents of the model neuron and integrated. Meanwhile, the membrane potential of the model cell is used to calculate the activation of the math-to-live synapse, and the membrane potential of the living cell is used to calculate the driving force of the current. The value of the

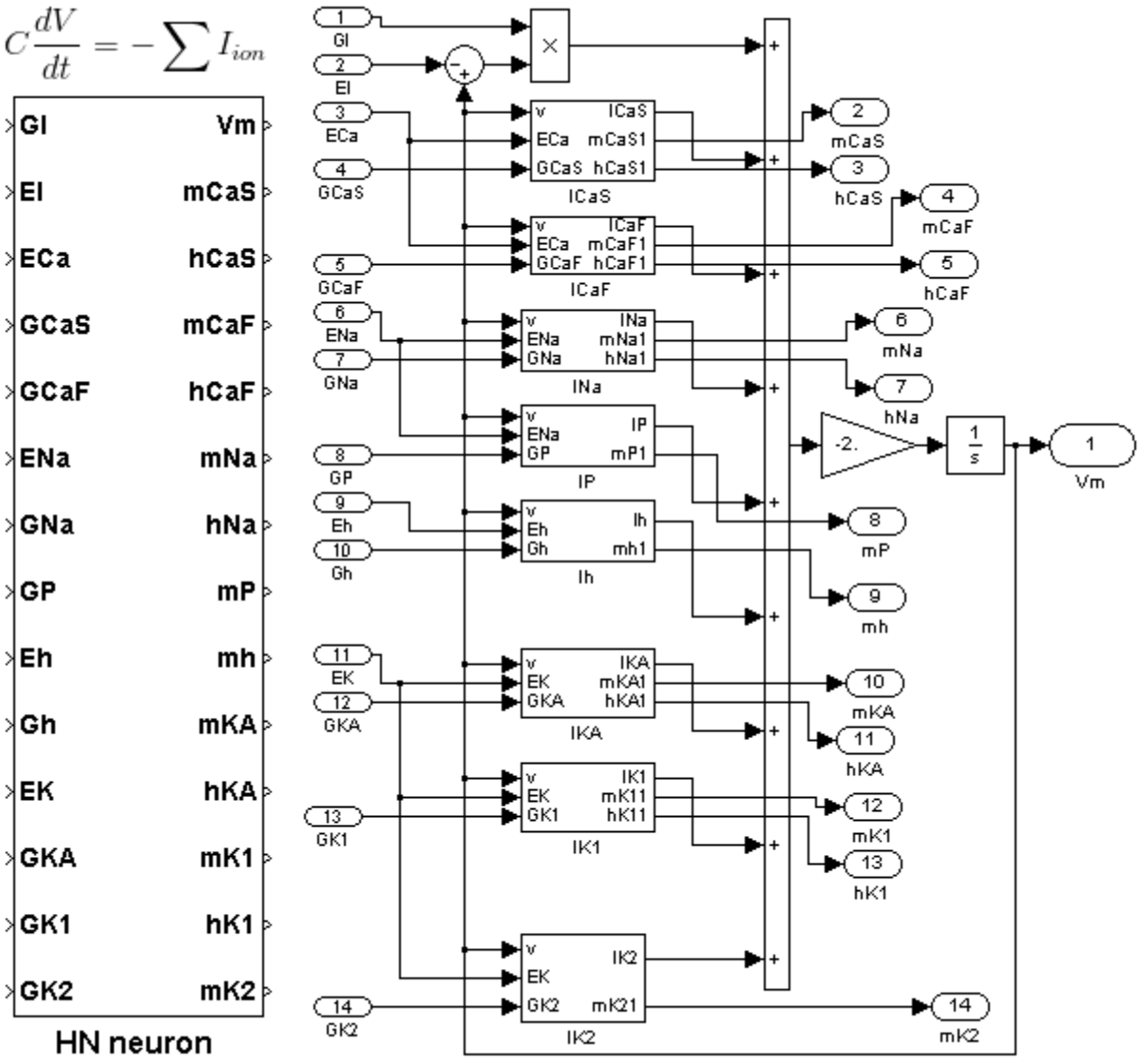

Figure 4. **Neuronal model.** This is the model hierarchical level: no system functions or state variables are calculated at a higher level. Each of the eight voltage gated currents is implemented as a subsystem block to keep the flow of the program uncluttered and allow maximum utilization of generic library functions. Conductance and reversal potential parameters are assigned at and each of the state variables are passed out to a higher organizational level for ease of access in ControlDesk.

current is passed into the DAC block, and the signal is fed from the CP1104 board into the injected current command port on the amplifier.

Building Neuronal Models with Simulink for Real-time Systems

Consider the model of the squid giant axon (Hodgkin & Huxley, 1952). It includes a fast sodium current (I_{Na}), a delayed rectifier potassium current (I_K), a leak current (I_L), and an injected current (I_{inj}). The differential equation for membrane potential takes the form

$$\frac{dV}{dt} = \frac{1}{C}\left[I_{inj} - \bar{g}_K n^4[V - E_K] - \bar{g}_{Na} m^3 h[V - E_{Na}] - \bar{g}_L[V - E_L]\right],$$

where the gating variables are defined as the differential equations

$$\frac{dn}{dt} = \alpha_n[1 - n] - \beta_n n, \qquad \frac{dm}{dt} = \alpha_m[1 - m] - \beta_m m, \qquad \text{and } \frac{dh}{dt} = \alpha_h[1 - h] - \beta_h h,$$

and the rate functions are

$$\alpha_n = \frac{10 \cdot [10 - V]}{\exp\left(\frac{[10 - V]}{10}\right) - 1}, \qquad \beta_n = 125 \cdot \exp\left(\frac{-V}{80}\right), \qquad \alpha_m = \frac{100 \cdot [25 - V]}{\exp\left(\frac{[25 - V]}{10}\right) - 1},$$

$$\beta_m = 4000 \cdot \exp\left(\frac{-V}{18}\right), \qquad \alpha_h = 70 \cdot \exp\left(\frac{-V}{20}\right), \qquad \text{and } \beta_h = \frac{1000}{\exp\left(\frac{[30 - V]}{10}\right) + 1},$$

such that V is the membrane potential, n is the activation of the potassium current, m is the activation of the sodium current, and h is the inactivation of the sodium current. The maximal conductance of an ionic current and its reversal potential are $\bar{g}_{ion}$ and E_{ion}. The parameter values used for maximal conductances are $\bar{g}_K$ = 36 mS/cm^2, $\bar{g}_{Na}$ = 120 mS/cm^2, $\bar{g}_L$ = 0.3 mS/cm^2, and the values used for reversal potentials are E_K = -12 mV, E_{Na} = 115 mV, and E_L = 10.13 mV.

Hodgkin-Huxley style neuronal models typically share a common structure. Gating variables are defined by voltage dependent rate functions, currents are defined by gating variables, and the membrane potential is computed by integrating the sum of the ionic

currents. The equations at each level of a model are often identical apart from numerical parameter values. Instead of building identical Simulink block diagrams for many functions in multiple currents, we choose to make block diagrams as generic as possible. If custom parameter values can be passed into different iterations of a single subsystem block, then that same block can be used to build more than one gating variable or ionic current. With this copy-and-paste style of programming, it is easy to compile libraries of multipurpose functions.

The dynamics of the squid giant axon model are determined by three channel opening rates and three channel closing rates. The reader will notice that of the six rate functions, there are only three unique equations. We have defined three functions such that each of the rate functions can be defined by choosing a function and providing the correct set of parameters: $k_1(c, d, V) = \frac{c[d-V]}{\exp\left(\frac{[d-V]}{10}\right)-1}$, $k_2(c, d, V) = c \cdot \exp\left(-\frac{V}{d}\right)$, and $k_3(c, d, V) = \frac{c}{\exp\left(\frac{[d-V]}{10}\right)+1}$. The functions $k_1(c, d, V)$, $k_2(c, d, V)$, and $k_3(c, d, V)$ are embedded in the subsystem blocks k_1 , k_2, and k_3 with input ports for c, d, and the membrane potential (Figure 5). Block k_1 corresponds to rates α_n and α_m; block k_2 corresponds to rates β_n, β_m, and α_h, and block k_3 corresponds to the rate β_h.

These rate functions and their associated parameters identify the otherwise generic gating variable derivative blocks. The gating variable blocks are used in much the same way; once the correct rate function and parameters are assigned, the derivative block can be dropped directly into the model. For example, the block dn%dt computes $\frac{dn}{dt} = \alpha_n[1 - n] - \beta_n n$. At this level of organization, the derivative block calls the rate function blocks k1 and k2 and assigns the rate parameters for α_n and β_n (Figure 6). It uses the

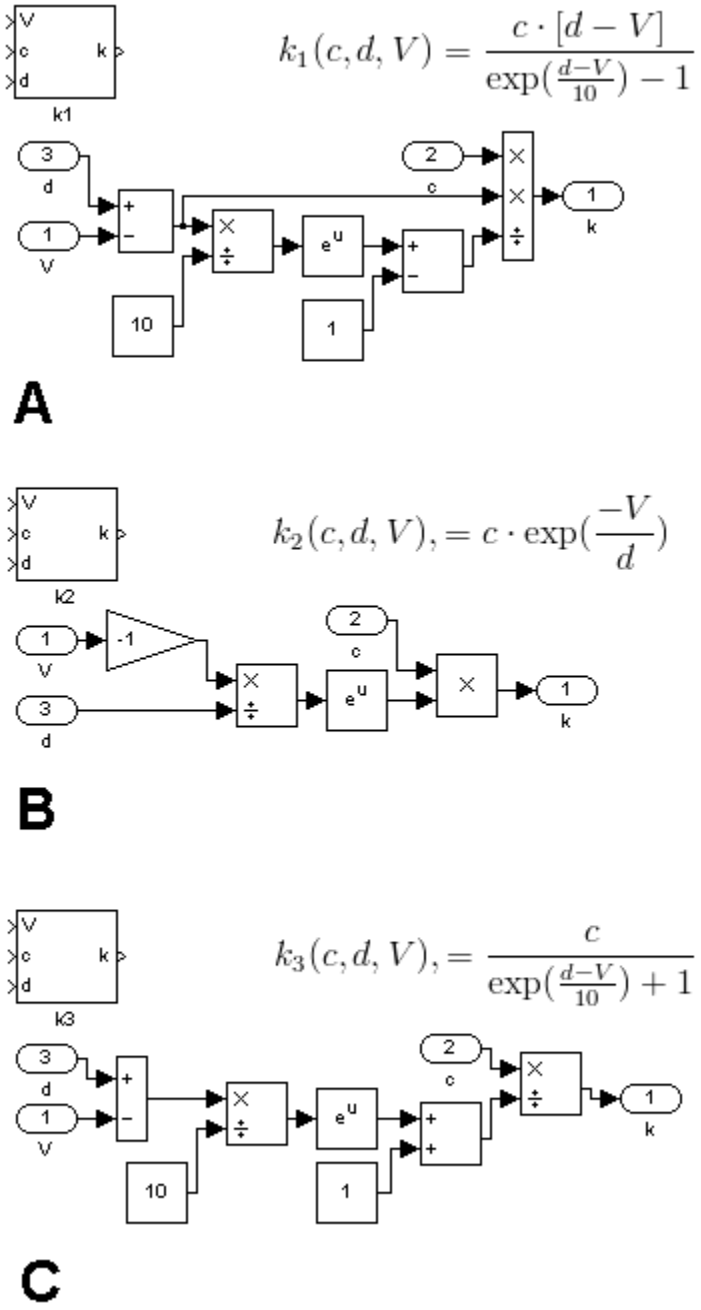

Figure 5. **Rate functions.** Each of the six rate equations takes the form of one of three equations differing only in parameter values. With just three unique subsystem blocks, all six of the rates can be implemented in Simulink. (A) The block *k1* represents function $k_1(c,d,V)$. This block is used for the rates α_n and α_m. Block *k2* represents function $k_2(c,d,V)$ which corresponds to rates β_n, β_m, and α_h. (C) Subsystem block *k3* represents the function $k_3(c,d,V)$ which corresponds to β_h.

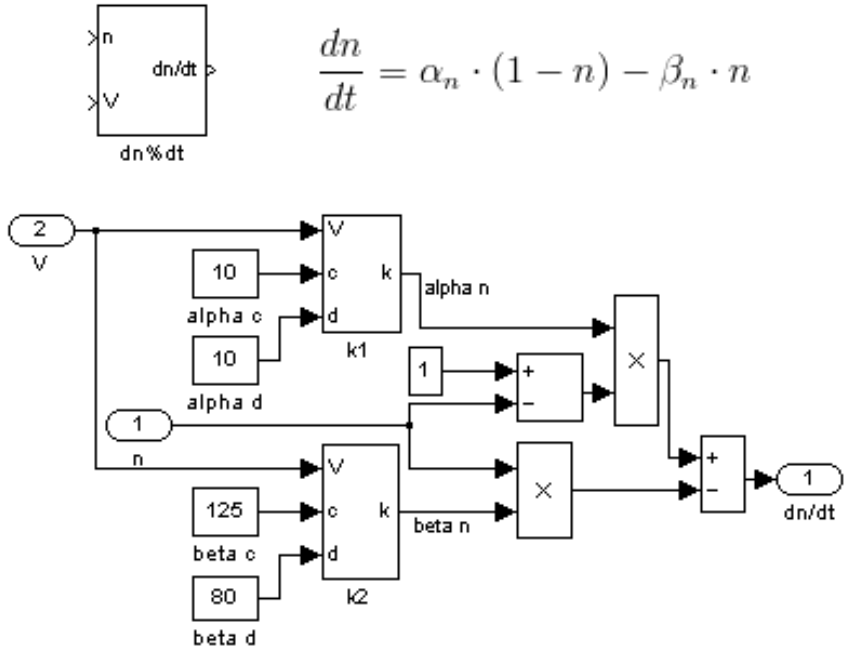

Figure 6. **Derivative equations.** The maximal conductance of a current is determined by the component gating variables. The temporal characteristics of each of these gating variables are determined by a pair of rate functions. The rate function blocks are inserted into a generic derivative block, and the parameter inputs are specified. Take, for example, the $dn\%dt$ block. Blocks k_1 and k_2 are the appropriate rate equations for α_n and β_n, and the rate parameters

current gating variable and membrane potential value to evaluate these functions and outputs the derivative of the gating variable with respect to time. Ionic current computation is a parallel process to gating variable computation in this model. The equations governing the conductances of the ionic currents are largely unique, so there is a dedicated box for each current.

In this model, integration is performed as a vector operation. The derivatives of each of the variables of state are multiplexed into a single signal and passed into the integrator. In the block diagram, the multiplexed signal is a darker connecting arrow (Figure 7). The actual operation of integration is performed on each derivative independently. There are

many methods for numerical integration. The simplest method is Euler's algorithm where, given some initial value of a function F, the derivative of the function is evaluated at discrete intervals of time in order to produce a numerical approximation of F as it evolves over time. Other methods may produce a more accurate approximation but often require that the function's derivative be evaluated many times for

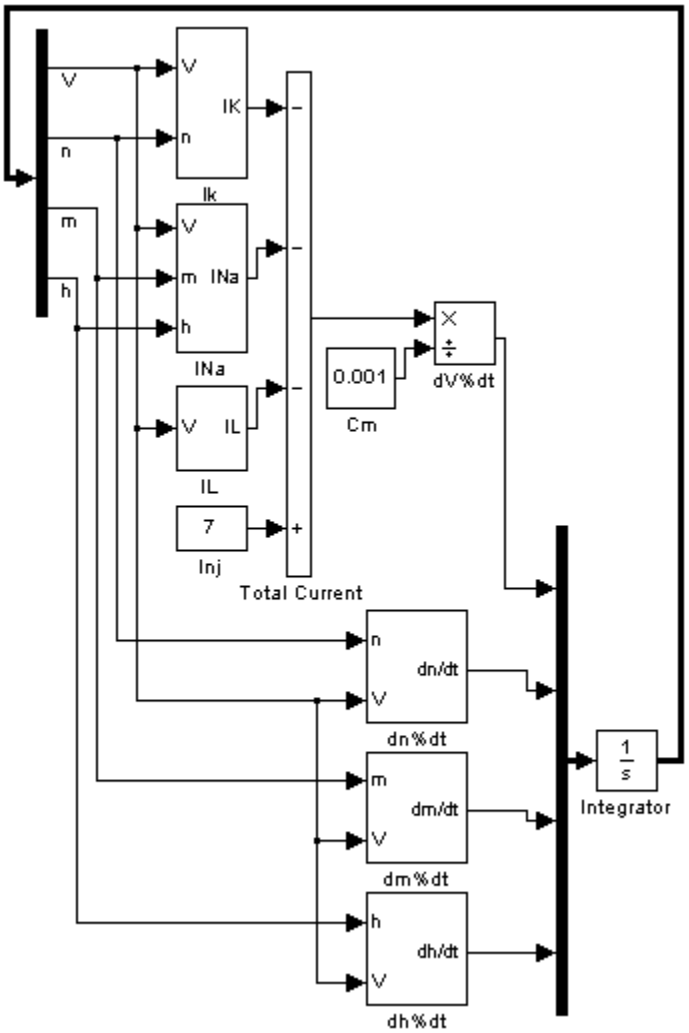

Figure 7. **Hodgkin-Huxley model.** The Hodgkin-Huxley model of the squid giant axon implemented as a block diagram. The variable derivatives are multiplexed onto one signal, and the system is integrated as a vector. The resultant state variables are demultiplexed and passed into the system. Rather than multiple Integrator blocks operating at different hierarchical levels, integration is carried out at the model level of organization. Dark upright blocks are multiplexers and demultiplexers. Thick connecting arrows indicate multidimensional signals.

each iteration of integration. These methods may be undesirable for real-time simulation because of time constraints on the algorithm.

Propensity to Hazardous Dynamics

For the parameter values provided by Hodgkin and Huxley, this model does not exhibit membrane potential oscillations. Brief depolarizing injected current pulses may elicit individual action potentials, and a constant depolarizing injected current may bring the cell into a regime of tonic firing. Moreover, for I_{inj} of sufficient amplitude, there exists a stable stationary state separated from the spiking regime by a stable manifold of a saddle type orbit (Guttman et al., 1980). Additional pulses of current may push the trajectory of oscillations beyond this orbit such that the membrane potential converges to the stable stationary state (Figure 8 A). Conversely, a current pulse of sufficient amplitude may push the trajectory outside of the basin of attraction of the stationary state, leading to membrane excitation and tonic spiking (Figure 8 B). This scenario can be tested by applying episodes of noise to the artificial Hodgkin–Huxley neuron.

First, though, we introduce a mechanism through which a model can interact with external processes. The dSpace PCI board will host the model, and its data acquisition channels will be available. Conveniently, the basic Simulink blocks and the dSpace data acquisition blocks may all be compiled to run in real-time. The DS1104MUXADC block reads input from the first four analogue to digital channels on the CP1104. This block will supply the noisy stimulus current used to switch the model from spiking to silence. The ADC block feeds directly into a gain block, so that the noise signal can be amplified to sufficient magnitude and is also modified by an offset current to keep the ambient stimulus signal at zero.

After the model is compiled with Real Time Workshop, it is loaded onto the dSpace board. We provide an example ControlDesk layout, *hazardhh.lay*, that contains tools to interact with and control the model in real-time. It includes a plot and control panel to monitor and capture the membrane potential and stimulus current. The layout also

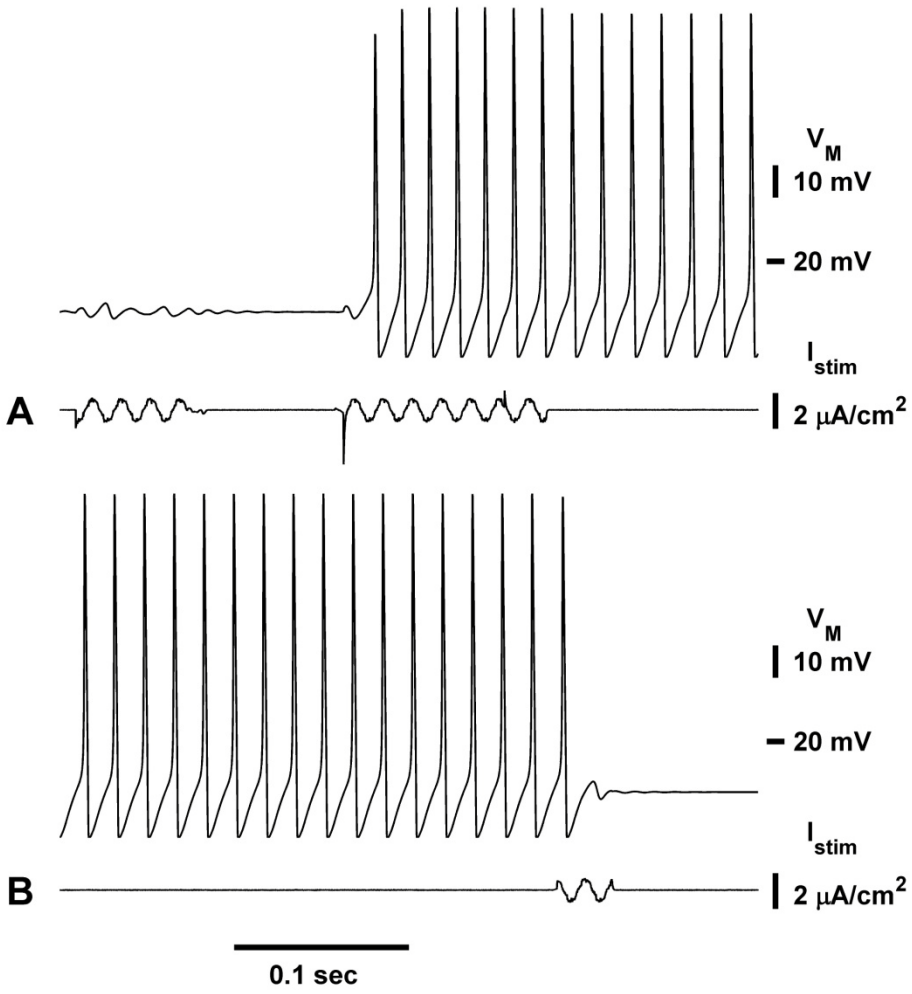

Figure 8. **Switching.** A stimulus current may cause excitation from silence to tonic spiking or cause the annihilation of tonic spiking. (A) Stimuli fail to and then succeed in pushing the trajectory outside the unstable orbit. The model cell transitions from silence to spiking. (B) A brief stimulus pushes the trajectory inside the unstable orbit; tonic spiking collapses onto the stable fixed point.

includes two numerical input fields to control the amplitude of the stimulus current and the offset current. It may be necessary to zero the ambient stimulus current by adjusting the offset block so that a baseline stimulus current does not modify the dynamics of the cell. We found our input to be balanced with an amplitude gain of 200 and an offset current at 1.5.

Using a conducting pin or wire, carefully touch the ADC1 port on the CP1104 and monitor the voltage and current traces in ControlDesk. As long as contact with the port is maintained, noisy excursions should be observed in the stimulus current. Notice that by simultaneously touching the electrode and the surrounding shield, a different waveform is produced. If initial contact with the electrode does not produce switching behavior, repetitive tapping may be sufficient, or it may be necessary to change the stimulus amplification and readjust the offset current (Figure 8).

4. PHARMACOLOGICALLY REDUCED LEECH HEART INTERNEURON

Motivation

The model {I_{Na}, I_{K2}, I_h} is based on a previously published model (Cymbalyuk & Calabrese, 2001; Shilnikov & Cymbalyuk, 2005). In order to reduce the mathematical complexity of the system, we simulate the activity of a heart interneuron in bath with Co^{2+} and 4-aminopyridine (4-AP). Application of Co^{2+} blocks Ca^{2+} currents and the synaptic current. Application of 4-AP blocks most of the K^+ currents. The remaining currents in this model are the leak current (I_L), the slow outward potassium current (I_{K2}), the fast sodium current (I_{Na}), and a constant polarizing current. Our model also includes the hyperpolarization activated current (I_h) which is present in this pharmacological scenario but has not been previously represented in reduced models. Intracellular recordings in these conditions show slow seizure-like oscillations with periods that are tens of seconds long (Opdyke & Calabrese, 1994).

The membrane potential (V) and each of the ionic currents are modeled using Hodgkin-Huxley formalism. The gating variables are the activation of I_{K2} (m_{K2}), the inactivation of I_{Na} (h_{Na}), and the activation of I_h (m_h). The activation of I_{Na} is taken to be instantaneous. It is modeled as the steady state curve of the activation of the current which is a function of V. The steady state curves of m_{K2} and h_{Na} are also sigmoidal functions of V, and the steady state of m_h is a modified sigmoidal curve. The time constants of m_{K2} and h_{Na} are constant, and the time constant of m_h is a function of V. The half activation value of a sigmoid function of V is the value of V at which the value of the function is one half. The half activation parameters for the activation of I_{Na} and h_{Na} are not varied. The half activation parameters of m_{K2} (θ_{K2}) and m_h (θ_h) are our control parameters.

$$\frac{dV}{dt} = -2[g_{K2}m_{K2}^2[V - E_K] + g_{Na}\left[\frac{1}{1+\exp(-150[V+0.0305])}\right]^3 h_{Na}[V - E_{Na}]$$

$$+g_h m_h^2[V - E_h] + g_l[V - E_l] + 0.006],$$

$$\frac{dm_{K2}}{dt} = \frac{\frac{1}{1+\exp(-83[V+\theta_{K2}])} - m_{K2}}{0.9},$$

$$\frac{dh_{Na}}{dt} = \frac{\frac{1}{1+\exp(500[V+0.0325])} - h_{Na}}{\tau_{Na,}},$$

$$\frac{dm_h}{dt} = \frac{\frac{1}{1+2\exp\left(180[V+\theta_h]\right)+\exp(500[V+\theta_h])} - m_h}{0.7+\frac{1.7}{1+\exp(-100[V+0.073])}},$$

The slow variables in this system are m_{K2} and m_h with time constants of approximately one and two seconds. As such, the temporal characteristics of these variables are instrumental in the dynamics of bursting activity. By systematically manipulating parameters that determine the dynamics of the slow variables, we can observe the range of bursting activity and bifurcations between qualitatively distinct regimes of neuronal activity. Bifurcation theory allows us to make predictions concerning the temporal characteristics of the dynamics of bursting nearby the critical transitions associated with the onset of bifurcation.

Bifurcation analysis of the model {I_{Na}, I_{K2}, I_h} was performed by shifting the half activation values of the two slow variables from the canonical values. While systematically varying these parameters, we observed the periodicity of bursting activity. The period of bursting activity is the time measured from the first spike of one burst to the first spike of the next. The burst duration is the time measured from the first spike of a burst to the last spike of that burst. The interburst interval is the time measured from the last spike of a burst to the first spike of the next burst, and the duty cycle is the ratio of burst duration to burst period.

Roles of I_{K2} and I_h

We established the role I_{K2} plays in supporting bursting activity in a model lacking I_h. Shilnikov and Cymbalyuk (2005) showed that as the half activation parameter approaches a critical value at the border of bursting and tonic spiking, the burst duration grows in accordance with a saddle node for periodic orbits while the interburst interval remains largely unchanged. By shifting the half activation voltage away from the border of bursting and tonic spiking, we observed a range of bursting that is approximately 0.006 V. Bursting activity at the lower end of this range consisted of long bursts interrupted by short interburst intervals, but activity for larger values of θ_{K2} consisted of short bursts with long quiescent phases (Figure 9A).

Bursting activity transitions to tonic spiking at the border of bursting for lower values of θ_{K2}, and bursting activity transitions to quiescence at the border of bursting for higher values of θ_{K2}. We analyzed the evolution of activity with changes in θ_{K2} by comparing the temporal characteristics of successive simulations (Figure 9B). Shilnikov and Cymbalyuk (2005) showed that for values of θ_{K2} where the burst duration was very sensitive to changes in the control parameter, the interburst interval remained constant. Similarly, we observed that for values of θ_{K2} where interburst interval of bursting activity was sensitive to θ_{K2}, the burst duration remained constant. Over the entire observed range of bursting, the spike frequency at the end of the burst fell between 5.4 and 5.7 Hz.

We introduced I_h and studied its role in bursting activity. The initial values we chose for θ_{K2} and θ_h were -0.0006 and 0.047 V respectively. At these values, we observed bursting

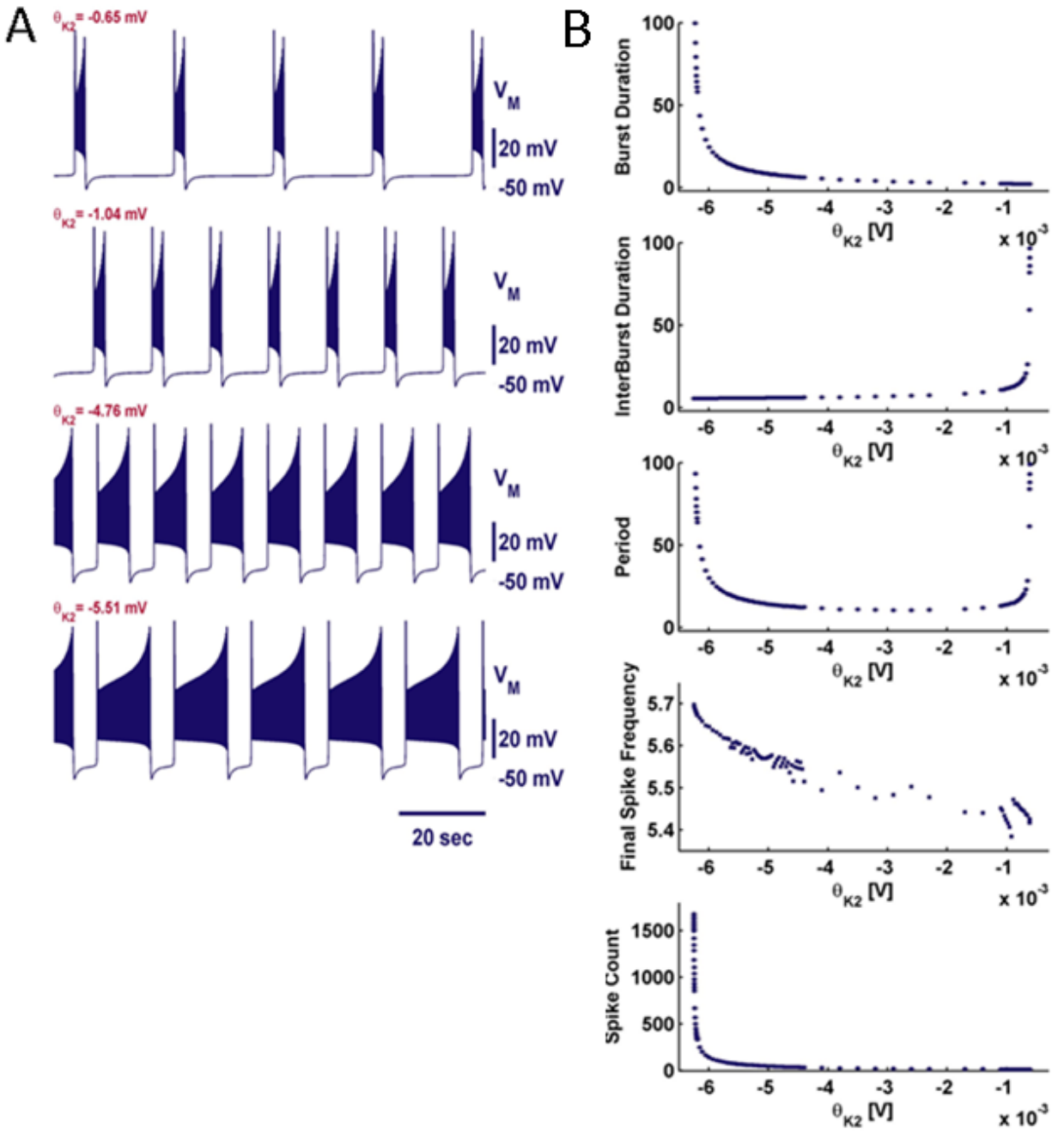

Figure 9. **Examples of activity and temporal characteristics while varying θ_{K2}.** (A) Example trajectories over a 0.005 V range for θ_{K2}. The burst duration is larger for lower values of θ_{K2}, and the interburst interval is larger for lower values of θ_{K2}. (B) Temporal characteristics for trajectories computed at different parameter values. The period of bursting has a U-shaped dependence on θ_{K2}. Growth in burst duration is due to spike addition. Large jumps in final spike frequency correspond to spike addition or spike deletion events.

trajectories with burst durations and interburst intervals of approximately 2 seconds (Figure 10). By varying θ_h, we observed bursting over a range of 0.06 V. We found that I_h primarily modulated the interbust interval in this model (Figure 11A). At the border of bursting for lower θ_h (-0.004 V) we observed a transition to depolarized silence. At the border of bursting at θ_h=0.056 V, bursting transitioned to hyperpolarized silence. As θ_h approached the lower border for bursting, the burst duration roughly tripled and became irregular from burst to burst (Figure 11B). As θ_h approached the upper border of bursting, the interburst interval became very large. In both cases, either the burst duration or interburst interval was sensitive to changes in θ_h while the other remained roughly constant. Similar to the previous system, the final spike frequency fell in a narrow range as we varied θ_h.

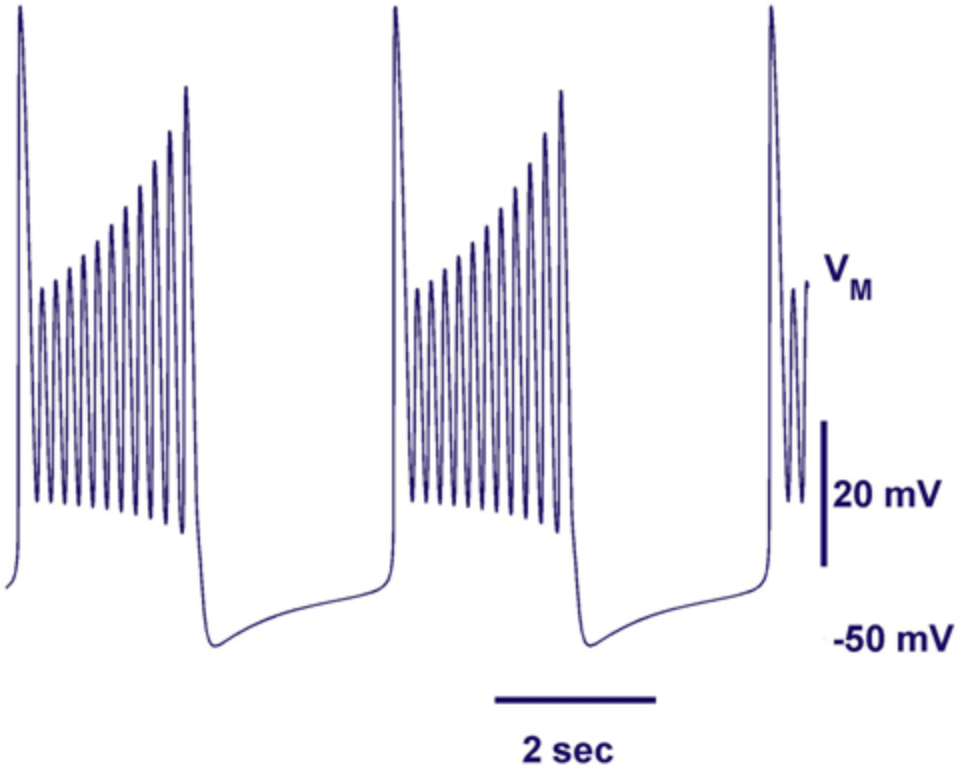

Figure 10. **Sample trajectory**. Burst duration and interburst interval are approximately 2 seconds for θ_{K2}= -0.0006 V and θ_h=0.047 V.

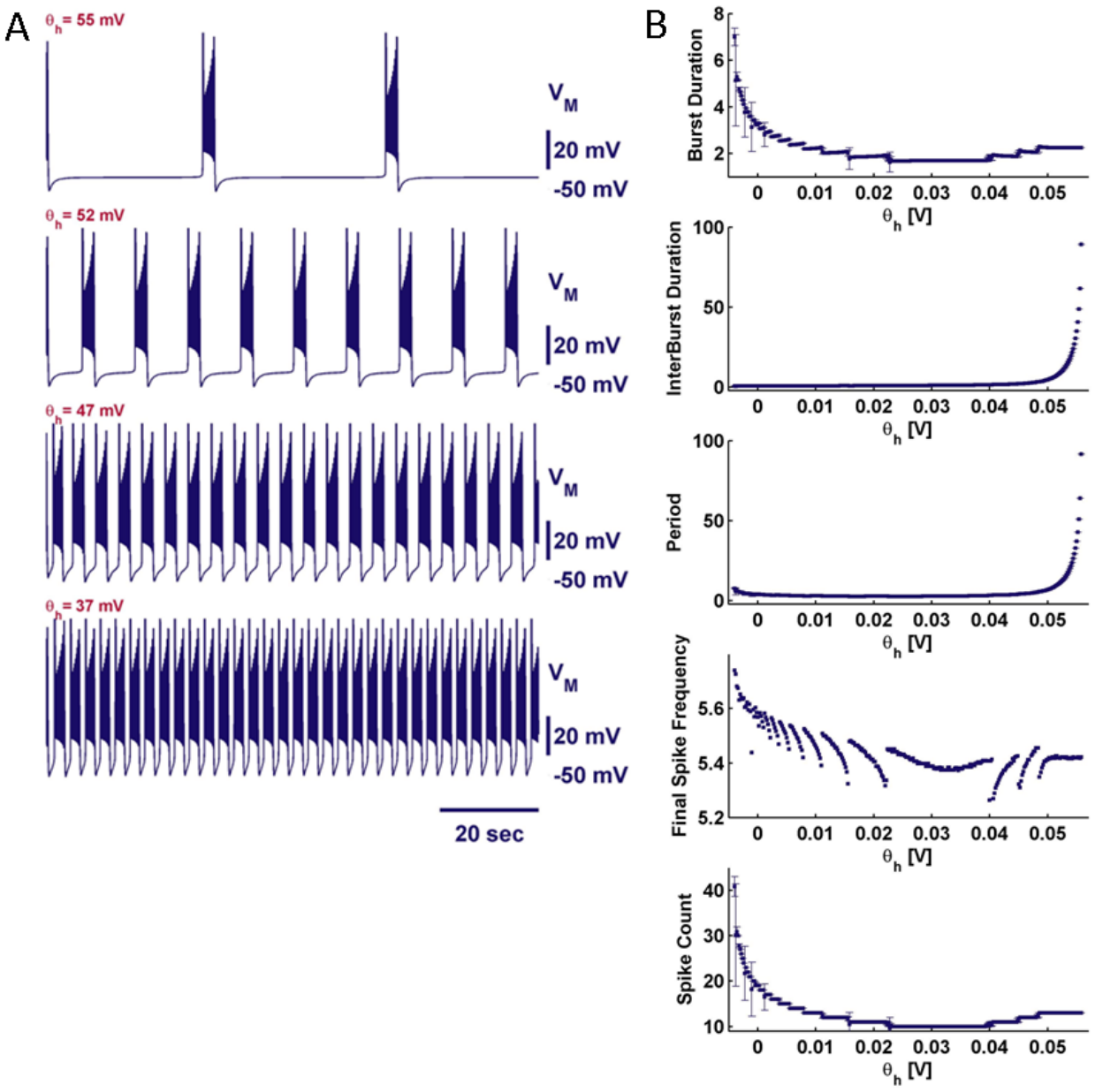

Figure 11. **Examples of activity and temporal characteristics while varying θ_h.** (A) Example trajectories over a range of values for θ_h. (B) Temporal characteristics for trajectories computed at different parameter values. Trajectories with irregular burst durations can be identified by the large standard deviations. Large jumps in final spike frequency correspond to spike addition or spike deletion events.

5. MAINTENANCE OF DUTY CYCLE

We used curve fitting to determine the laws that governed the evolution of temporal characteristics as bifurcation parameters approach critical values. Once identified, these laws allowed us to characterize the type of bifurcation the system undergoes at the critical value. Numerical methods allowed us to characterize the type of and compute parameter space coordinates for these bifurcations directly. We were able to re-characterize the control parameter of bifurcation as the distance along a line made up of points in the parameter space sharing the same duty cycle.

Saddle-node Bifurcation

A saddle-node bifurcation for stationary states occurs when a fixed point is born, and separates into two fixed points. In the one dimensional case, a semi-stable fixed point separates into a stable and an unstable fixed point. In the case of two or more dimensions, a saddle-node is born and separates into a saddle and a node. In the case where a saddle-node bifurcation occurs on an orbit, the orbit dies on the fixed point. It is possible to detect the approaching bifurcation by observing changes in the period of the orbit. For a given variable q, the derivative of q with respect to time approaches zero for a certain phase of the orbit as the bifurcation parameter *x* approaches a critical point *c*. As such, the orbit slows down when it passes near this bottleneck. As *x* approaches *c*, the period increases proportionally to one over the square root of the difference between the critical point and the control parameter: $T = a/\sqrt{(x - c)}$.

The fold limit cycle is similar to the saddle-node bifurcation for stationary states, but pertains to the birth of limit cycles. As the bifurcation parameter changes, a saddle periodic orbit is born; it promptly splits into a stable and an unstable cycle. Trajectories that pass

near a fold limit cycle experience a bottle neck in a similar way as trajectories that pass near a saddle-node for stationary states. Rather than spending more and more time nearby the stationary state, trajectories spend more and more time oscillating nearby the saddle periodic orbit. The period of these trajectories grows proportionally to one over the square root of the control parameter. This has been reported previously for the first example in the previous chapter (Shilnikov & Cymbalyuk, 2005). We observed a saddle-node bifurcation for stationary states for both cases presented in the previous chapter. As θ_{K2} is varied towards the border of bursting and silence and θ_h is varied towards he border of bursting and hyperpolarized silence, the interburst interval of each grows in accordance to the saddle-node bifurcation (Figure 12).

Control of bursting activity through coregulation of slow currents

We observed the behavior of the system by extending our analysis onto the plane of θ_h and θ_{K2}. The parameter θ_h was varied from -0.153 V to 0.147 mV, and θ_{K2} was varied from -0.025 V to 0.010 V. For every value of θ_h observed, there was a finite window in θ_{K2} where bursting was possible. For values of θ_h above 0.010 V and below -0.053 V, changes in θ_h ceased to modulate bursting activity. When θ_h is above 0.057 V, θ_h drops below the range of bursting behavior. In other words, I_h activates below the lowest voltage in a burst, and the current is effectively shifted below the bursting activity. Further increases to θ_h are superfluous. Similarly, when θ_h is below -0.053 V, the curve for steady state of activation is close to one for the range of membrane potentials expected in a burst. In this case, I_h is always activated, and any further decrease in θ_h is inconsequential.

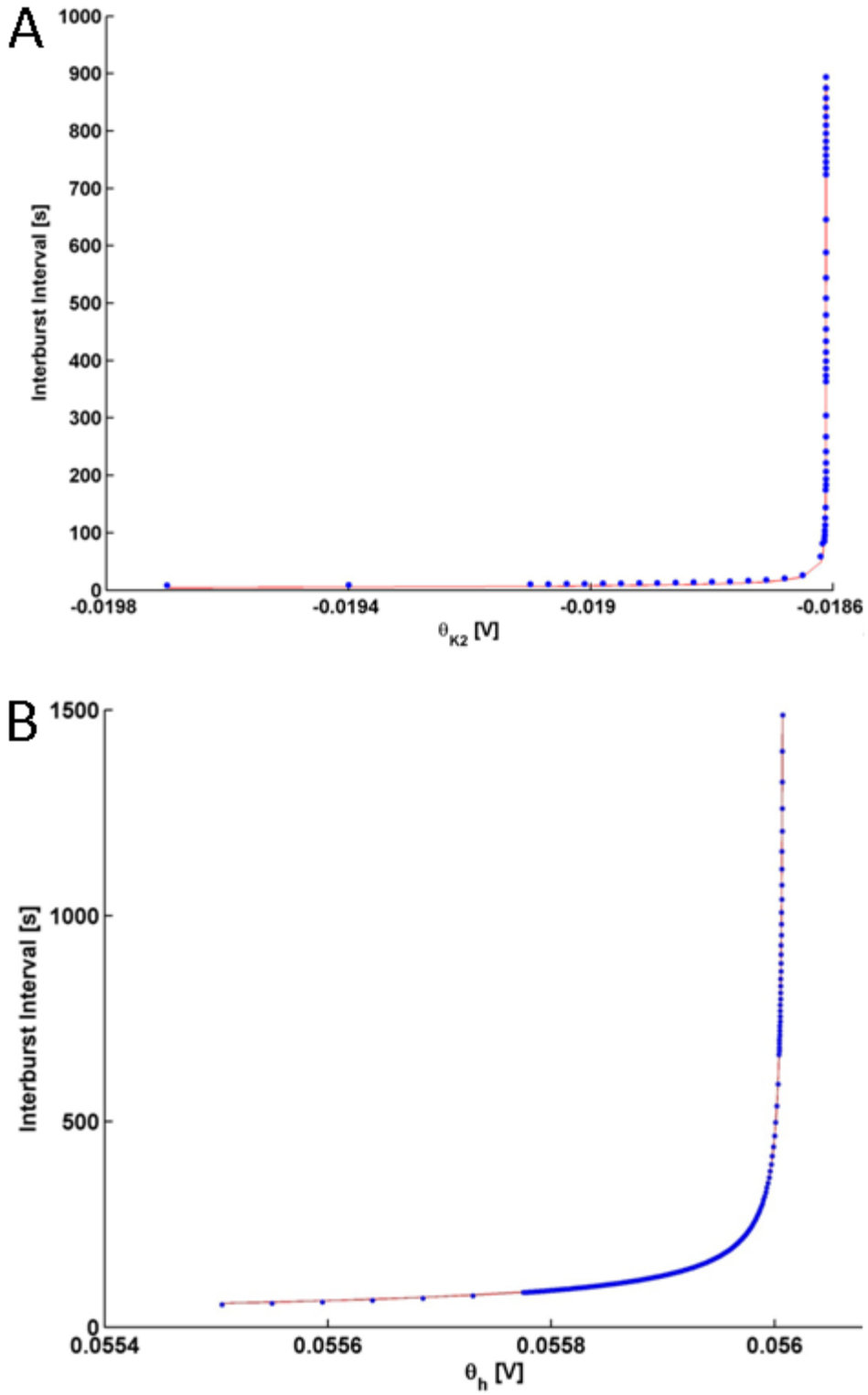

Figure 12. **Interburst interval plotted against θ_h**. The blue points represent values obtained from computed trajectories. The red curve is the plot of the function fitted to the data: (A) a=0.1454 and c=0.01861 (B) a=1.302 and c=-0.05601.

We observed a complicated relationship between the periodicity of bursting behavior and the half activation parameters θ_h and θ_{K2}. Changes in period over the parameter space were the result of variations in interburst interval and/or burst duration. The periodicity was generally characterized by two cases: above and below a line at roughly 0.057 V in θ_h. The period generally increased for values of θ_h approaching this line from below. Period also grew in this region as θ_{K2} decreased. The union of these two cases, where θ_{K2} was near the point of burst termination for negative values and θ_h was near 0.057 V, showed a very sharp increase in period observed to around 30 s. The region above the line at 0.057 V shows no change in period with any change in the parameter θ_h, and since the activation of I_h was so hyperpolarized, the system was effectively reduced to three dimensions. Bursting was observed between the fold limit
cycle and saddle-node bifurcations at -0.006 V and 0 V in θ_{K2}. As the bifurcation parameter approached either of these values, the period grew towards infinity.

As θ_{K2} decreased towards burst termination, the peak burst duration observed can be broken into categories that correspond to three ranges for θ_h: below -0.053 V, between -0.053 V and 0.057 V and above 0.057 V. Below -0.053 V in θ_h, burst duration was wholly on the order of half a second. In this region below θ_{K2} values of 0.008 V, burst duration was slightly longer on average but also became irregrular. Above –0.053 V in θ_h, the border of bursting behavior for lower values of θ_{K2} dropped to around -0.006 V at the line where θ_h was 0.057. Additionally, the burst duration at the border increased as θ_{K2} dropped and θ_h grew to the point where the border was defined by a fold limit cycle (Figure 13). Nearby this bifurcation, the period could be arbitrarily large. The burst duration increased

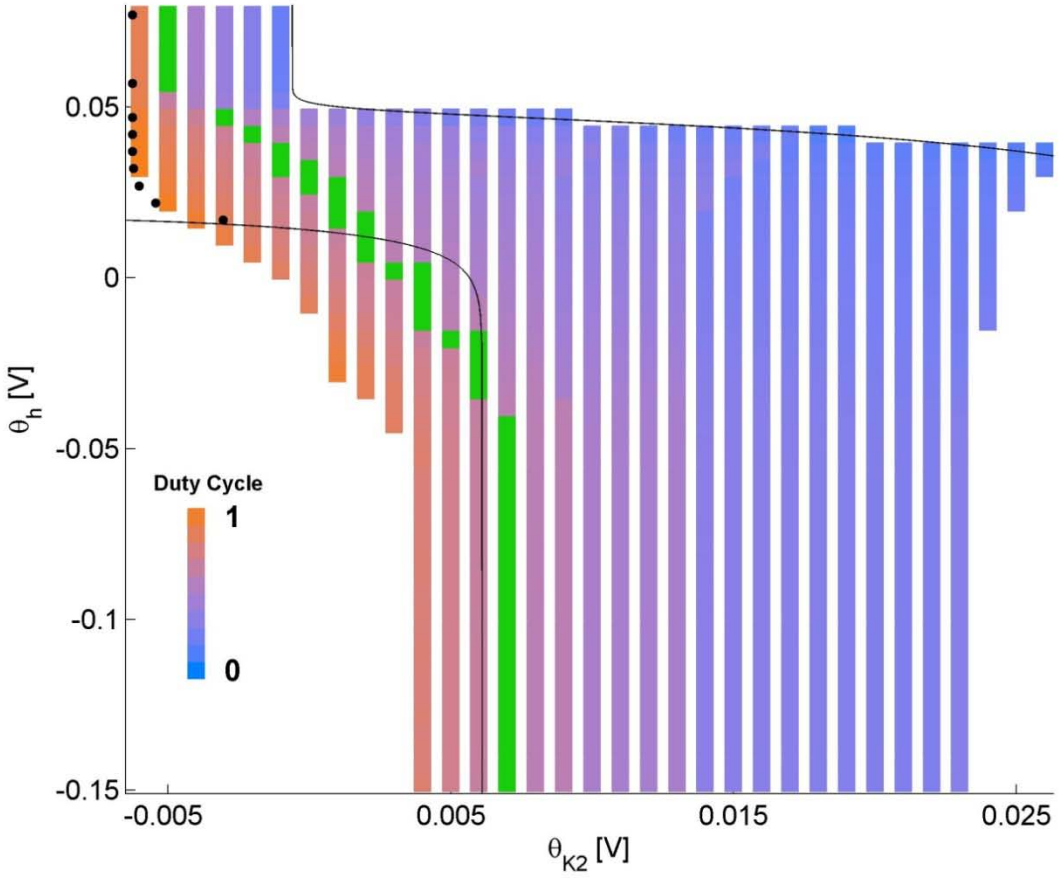

Figure 13. **Bifurcation diagram.** Points on the map corellate to values of θ_h and θ_{K2} for which bursting was observed. Warmer colors correspond to higher duty cycle, and cooler colors correspond to smaller duty cycle. Excluded from this rule are the series of green points which have a duty cycle between 0.55 and 0.60. The black dotted line corresponds to a fold limit cycle. The upper black line is a saddle-node bifurcation. The lower black line is an Andronov-Hopf Bifurcation.

monotonically to infinity as θ_{K2} approached the fold limit cycle for values of θ_h above 0.057 V.

Maintenance of Duty Cycle

Further analysis was performed by computing the duty cycle of bursting behavior (Figure 13). Duty cycle is the ratio of burst duration to period: a neuron that exhibits bursting activity with a period of 30 s and burst duration of 15 s has a duty cycle of 0.5. We

observed high duty cycles were bursting terminated at lower values of θ_{K2}. Duty cycle did not vary with θ_h for values above 0.057 V. For values of θ_{K2} close to the saddle-node bifurcation, the duty cycle approaches zero, and for values of θ_{K2} close to the fold limit cycle, the duty cycle approaches one.

For values of θ_h below -0.053 V, a similar trend was observed. Greater values for duty cycle were found at the lower border of bursting in θ_{K2}, and lower values for duty cycle were found at the upper border of bursting in θ_{K2}. In neither case were we able to achieve arbitrarily large or small duty cycles. Between values above -0.053 V in θ_h, the peak value for duty cycle followed the border of bursting as θ_h grew to 0.057. For coordinates in the parameter space nearby the lower border of bursting in this region, duty cycle decreased most rapidly for coordinates moving away from the border up to approximate value of 0.004 mV in θ_{K2}. Beyond this point, further changes in duty cycle were primarily dependent on θ_{K2}.

We observed subsets of data points for which duty cycle remained constant despite smooth growth in the period of bursting (Figure 14). We were able to further characterize the bifurcation diagram by limiting observation to a small range of duty cycle (green points in Figure 13). We found an apparently continuous curve of equal duty cycle that was linearly dependent on θ_{K2} and θ_h in the range between the saturation and removal of the activation of I_h. Above and below parameter values for which this saturation and removal occurred, equal duty cycle curves no longer varied with θ_{K2}.

Similar and congruent curves existed nearby in the parameter space for different duty cycles (Figure 15). Each curve is roughly parallel to the border of bursting defined by θ_{K2} on the left of the diagram, and the border of bursting defined by θ_h across the top of the

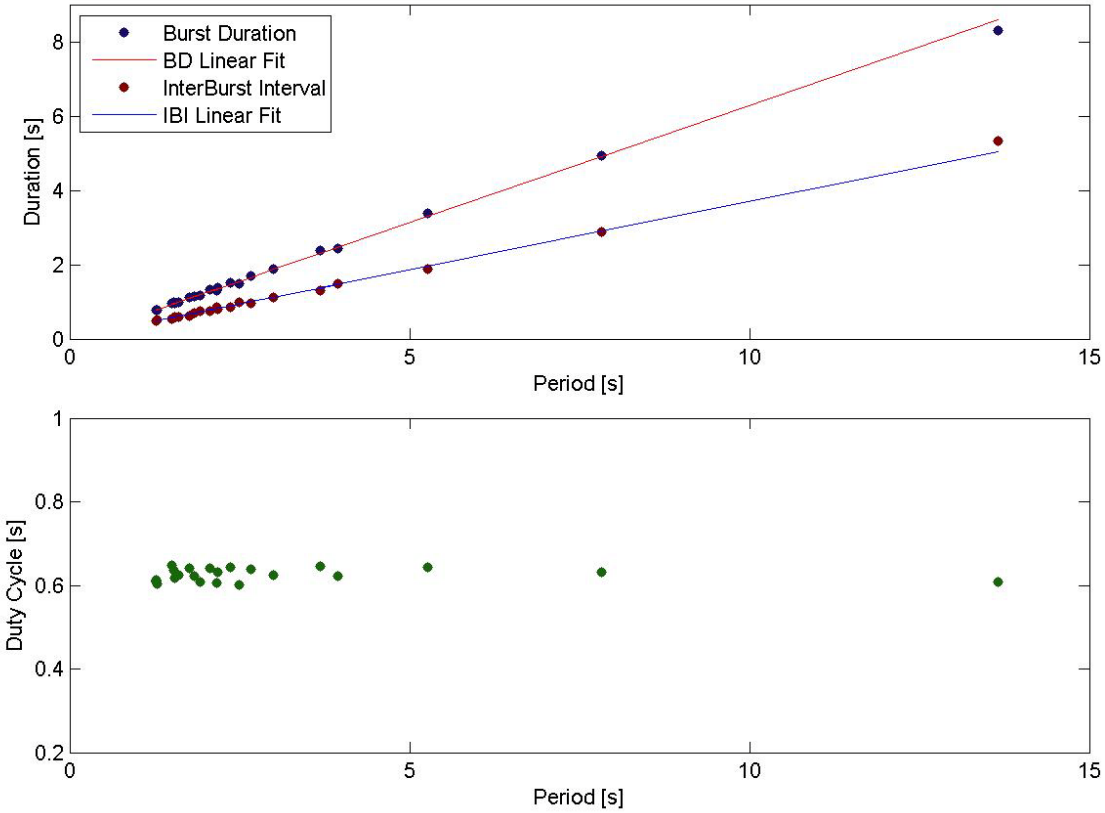

Figure 14. **Linear relationship.** Burst duration and interburst interval maintain a linear relationship with period. Duty cycle does not vary.

bifurcation diagram. These curves increased in period from the bottom of the bifurcation diagram where the activation of I_h is saturated to the top where I_h is no longer activated. Just as the period of bursting was no longer dependent on variations in θ_h above and below certain parameter values, the period along equal duty cycle curves no longer varied with θ_h above and below these values.

As each curve approached the point at which the activation of I_h is fixed at zero, the period grew proportionally to one over the square root of the distance along a curve of equal duty cycle (Figure 16). We characterized this distance by computing the distance of each data point along a linear fit line in the parameter space (Figure 15 and 16). The range

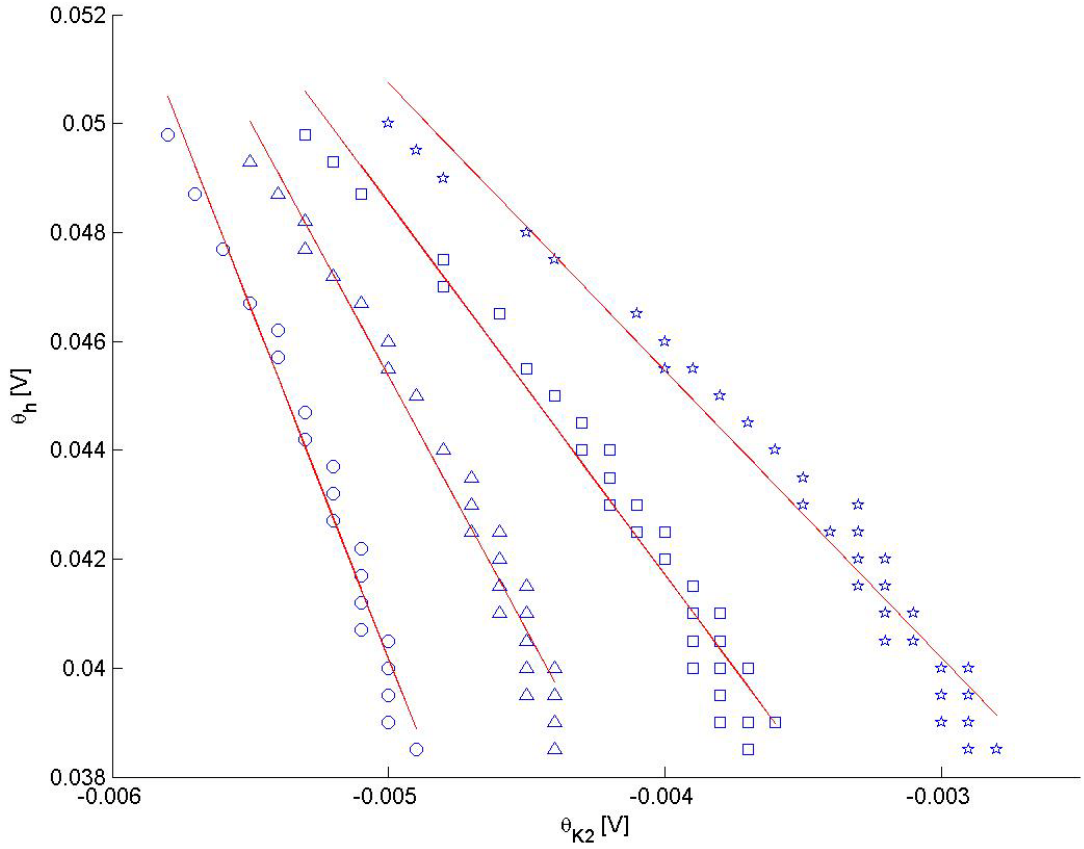

Figure 15. **Congruent lines.** We show four congruent lines of equal duty cycle. Each set of points was fitted to the form y=mx+b. The circular points correspond to a duty cycle between 0.81 and 0.8 and fitted to m=-12.91 and b=-0.304. The triangular points correspond to duty cycles between 0.76 and 0.75 and fitted to m=-9.374 and b=-0.217. The square points correspond to duty cycles between 0.71 and 0.7 and fitted to m=-6.854 and b=-0.156. The pentagonal points correspond to duty cycles between 0.66 and 0.65 and fitted to m=-5.274 and b=-0.118.

of bursting in parameter space contracts as I_h is shifted out of the bursting regime, and the period of bursting increases. The distance in parameter space from both the saddle-node bifurcation for stationary states, and the fold periodic orbit decreases with this contraction until I_h is no longer activated. Up to this point, trajectories on a line of equal duty cycle proportionally experience the ghost of both bifurcations so that burst duration and

interburst interval grow proportionally (Figure 14 and 16). Without compensation in I_h, the period cannot increase while duty cycle is maintained, and the bifurcations become entirely dependent on θ_{K2}.

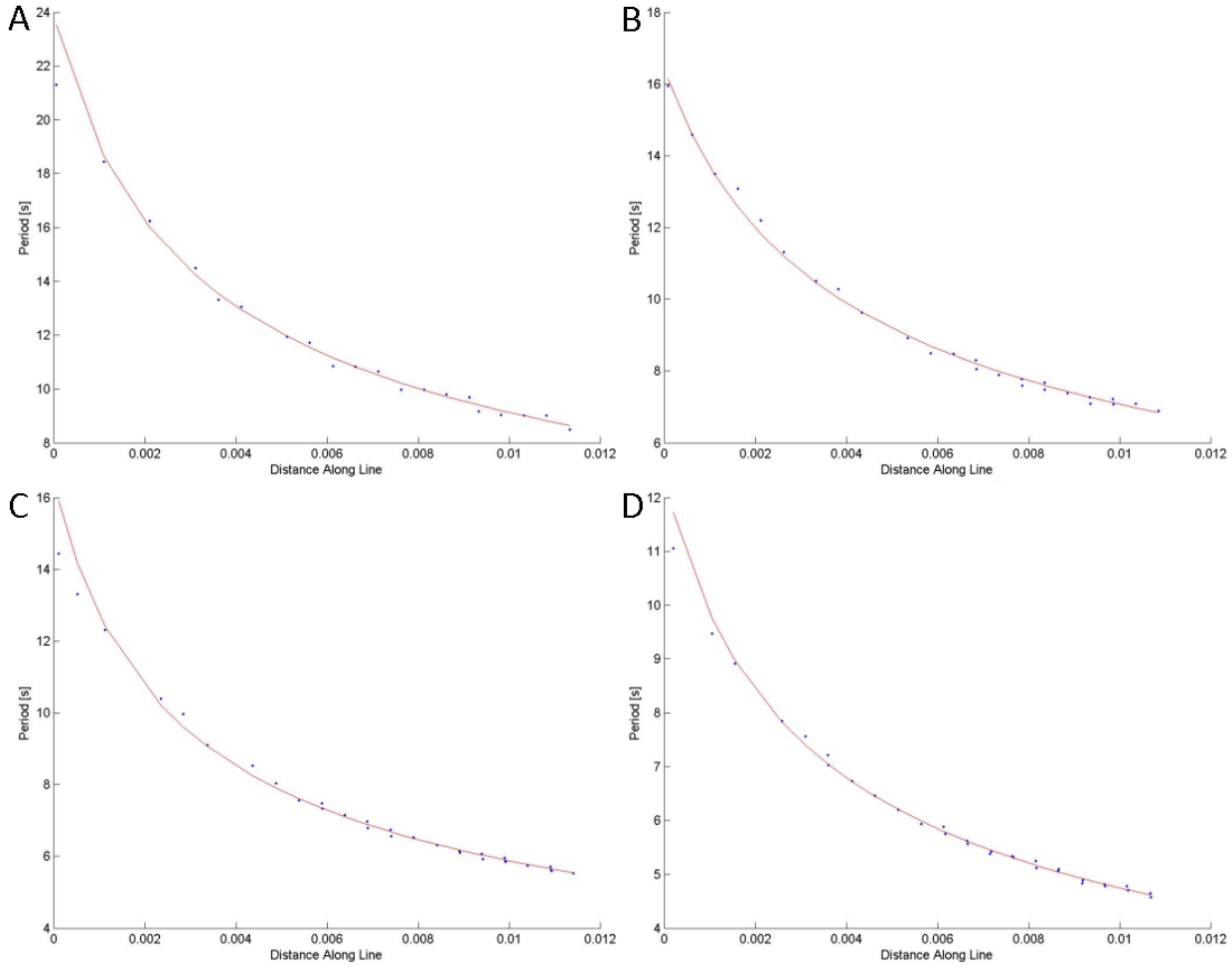

Figure 16. **Congruent curve fits.** Each set of points corresponds to a set of duty cycles, and a curve fit against the distance along the lines depicted in Figure 15. The distance of each point was computed by determining the projection of the data point onto the best fit line. The point with greatest period was considered the first point, and the euclidean distance of each point was measured from the first point. Each curve fit took the form $y=a/\sqrt{(x-b)}$. (A) Duty cycle is between 0.81 and 0.8. a= 0.988 and b=-0.002. (B)Duty cycle is between 0.76 and 0.75. a=0.784 and b=-0.002. (C)Duty cycle is between 0.71 and 0.7. a=0.629 and b=-0.001. (D) Duty cycle is between 0.66 and 0.65. a=0.514 and b=-0.002.

6. DISCUSSION

Our goal was to construct a biophysically plausible and biocompatible artificial neuron. We satisfied the real-time requirements of hybrid systems with Simulink's Real Time Workshop and dSpace hardware. We showed the preservation of a behaviorally critical characteristic, constant duty cycle, in a neuronal model.

Neuroprosthetic devices will one day routinely treat neurological disorders by monitoring and regulating the electrical activity in the central nervous system. Such brain-machine interfaces will need to be small, fast, and power efficient. The introduction of the analogue very-large-scale integration (aVLSI) neuron provides a framework for artificial cells and neural networks that satisfy these criteria (Mahowald & Douglas, 1991). Silicon neurons working in tandem with living networks have produced biologically valid patterns (Jung et al., 2001; Sorensen et al., 2004). The optimization of circuit design promises efficient and biocompatible VLSI chips (Rachmuth & Poon, 2008). The clinical distribution of these neuroprostheses will require industrial manufacturing of implants. Like any other industry, the neuronal models upon which these devices will be based will need to be tested before the production process begins. Testing could be done with a hybrid system: artificial neurons can be interfaced with biological neurons or networks of neurons with a dynamic clamp. By tuning characteristics of the artificial cell, an analysis of the hybrid system can reveal pathological or otherwise undesirable neuronal or network states. By prototyping neuroprostheses in this manner, a researcher can design an artificial cell that meets implant design parameters without compromising the dynamics of the biological component of the hybrid system.

In order for a hybrid system to function properly, the artificial system must be simulated on a computer such that computational cell is able to respond to the living cell without interruption. These computational necessities are often accomplished with real-time computing in which operations are performed on a strict schedule. While most modern desktop computers are capable of running real-time software, most modern operating systems are not real-time. Developers must rely on specialized products to implement real-time applications: a real-time operating system runs a program directly on the desktop computer or a program is run on a real-time peripheral device (a control board) that is controlled from the desktop computer. A prominent supplier of real-time control boards and support software is dSpace. dSpace products are commonly used for prototyping control systems in the robotics, automotive, and aerospace industries. dSpace software automatically utilizes a system designed in Simulink and executes it on a real-time control board. We realize hybrid systems by designing neuronal models in Simulink and using dSpace to implement these models in real-time.

Matlab & Simulink provide a high level programming language designed for technical and high performance computing. Simulink is a graphical programming environment; Simulink programs look like flow charts. Individual operations are represented as blocks, and blocks are connected with arrows showing how the output of one block is used by other blocks. Larger mathematical expressions may be contained by a single block so that, in our case, biophysical functions such as current, conductance, and driving force can each be represented as individual blocks. Even an inexperienced user can go from a set of equations or a conceptual flow chart to a sophisticated model quickly with

Simulink's drag-and-drop programming style. As in any high level programming language, program components can be reused to reduce development time.

We provide a library of functions in Simulink sufficient to create a neuronal model. This library includes individually implemented artificial currents, voltage dependent steady state curves, and voltage dependent time constants. Moreover, these functions provide a template with which to construct novel neuronal models. Many of our functions are standardized so that each numerical parameter is specified by the user. By providing custom parameters based on experimentally measured ionic currents, a researcher could implement any number of currents not found in our library. These models are designed to be used as real-time control systems for a dynamic clamp.

In order for a neuroprosthesis to assume the role of some functional neuronal circuit, it must behave as though it is a functional neuronal circuit. That means that it must continue to have a functional role in its host as the local and global neuronal environments change over time. Factors such as fatigue, age, injury, and drug use can all change the way neuronal circuits and their synaptic targets function. Prosthetic activity must be robust so that the larger neuronal circuit remains resistant to degeneration. We use the numerical and analytical tools of dynamical systems theory to study the mechanisms through which these environmental factors enact neuromodulation in order to identify manifestations of pathology in model neurons.

Dynamical systems theory provides a theoretical foundation for sensitivity analysis in mathematical models. Qualitative aspects of a dynamical system can be revealed through mathematical analysis of critical parameter values and initial conditions in the context of perturbations and environmental noise. For example, there may exist multiple stable

regimes nearby each other in state space (multistability), or the activity of a system may change dramatically with small changes to sensitive parameters (catastrophe). Nearby certain of these catastrophes, the behavior of a system will obey specific laws governing periodicity. Regimes of activity that exist in a multistable or potentially catastrophic system are hazardous: small perturbations to the system may cause the system to switch to a different mode of activity. Multistability and catastrophes are not mutually exclusive. A catastrophe may manifest itself as one of many stable modes becomes unstable or disappears. Forearmed with the knowledge of the type activity that can be expected across a range of parameters, a researcher may design a model neuron in order to exclude or take advantage of certain regimes.

Multistability and catastrophes can be used to describe several facets of intrinsic neuronal dynamics and modulation. A neuron may exhibit bistability of stable regimes (Guttman et al., 1980; Paydarfar et al., 2006; Shilnikov et al., 2005). Such a cell could toggle between coexistent states upon stimulation. Using dynamical systems theory, a researcher may predict such bistability in a neuronal model. If the model is intended to fire indefinitely as a pacemaking oscillator, then bistability would be a pathological trait. On the other hand, bistability could be a functional trait if the model is intended to be an on-off switch that modulates some macroscopic behavior. A model neuron may switch from endogenous bursting to tonic spiking at a particular parameter value (Cymbalyuk et al., 2002). A researcher may implement this parameter as a slow variable dependent on the model's synaptic input or state of activity in order to effect modulation of neuronal dynamics.

What distinguishes a model from a living cell is adaptation. The dynamics of specific neuronal processes, such as the activation of an ionic current, may be sensitive to the

behavioral state of that neuron. These activity-dependent processes in turn shape future neuronal activity states. This autoregulatory feedback allows a cell to maintain structural stability of functional regimes. Autoregulation is mediated by intracellular signals. A number of neuronal models exhibit long term neuromodulation based on intrinsic Ca^{2+} dynamics (LeMasson et al., 1993; Liu et al., 1994; Siegel et al., 1994). As long as functional behavioral regimes are stable, environmentally triggered excursions onto pathological regimes ultimately converge back onto more desirable solutions through the action of these characterizing variables. This model of neuromodulation lends itself to a hypothesis of homeostasis (Marder & Prinz, 2002).

Our model of the leech heart interneuron is a good candidate in which to study the role of modulation on and adaptation in a single cell. Parameters in Hodgkin-Huxley type models correspond to measurable characteristics of currents in living cells. By performing bifurcation analysis and continuation with characteristics that have been shown to change under neuromodulation, we may simulate the role of neuromodulation in neuronal dynamics. The half activations of hyperpolarization activated currents and potassium currents have been shown to vary in the presence of modulators (McCormick & Pape, 1990; Luthi & McCormick, 1998; Luthi & McCormick, 1999; Peck et al., 2001).

We performed parameter scans for temporal characteristics similar to Cymbalyuk et al. (2002). Previous studies, also with θ_{K2}, on similarly reduced models have shown blue-sky catastrophe and Lukyanov-Shilnikov transitions from bursting to tonic spiking (Shilnikov & Cymbalyuk, 2005; Shilnikov et al., 2005). The activation of I_{K2} supports bursting. I_h in our model clearly acts in a modulatory role; the neuron bursts whether I_h is activated or not. Between the two currents, we have control over burst duration with θ_{K2}

and interburst interval with θ_h. We have shown that cell intrinsic adaptation may change period while duty cycle remains constant and that a negative correlation in the regulation of the two half activation parameters is required to affect duty cycle maintenance. We have created a prototype with which to implement a biohybrid system. Using real-time technology and dynamic clamp, we can study the role of I_h and I_{K2} in the dynamics of a living corollary to our model neuron.

7. CONCLUSION

We developed a library of Simulink S-functions to efficiently model neuronal dynamics in real-time.

We developed and analyzed model of an artificial neuron representing the leech heart interneuron under specific pharmacological conditions.

We showed duty cycle maintenance could be achieved through coregulation of a hyperpolarization activated current and a potassium current. Negative correlation between the half activation voltages allows the artificial cell to keep the duty cycle constant independent of changes in period from 2 to 13 s.

PUBLICATIONS

Anquez M, Belen C, Harris T, Barnett W, Malashchenko T. Faculty sponsor G Cymbalyuk. Analysis of activities of leech heart interneurons: pushing limits between bursting and silence. Georgia State Undergraduate Research Conference (GSURC). March 13, 2009.

Barnett W, Anquez M, Cymbalyuk G. Modeling maintenance of duty cycle via covariation of two slow currents. 2010. In preparation.

Barnett W, Anquez M, Harris T, Cymbalyuk G. Control of epileptiform bursting in the leech heart interneuron. 76th Annual Meeting of the Southeastern Section of APS, November 2009, PC.00005.

Barnett W, Anquez M, Harris T, Cymbalyuk G. Modeling modulatory effects if Ih and INap on bursting of a leech heart interneuron. South East Nerve Net meeting, March 2009.

Barnett W, Cymbalyuk G. Hybrid Systems Analysis: Real-Time Systems for Design and Prototyping of Neural Interfaces and Prostheses. Chapter 8 in Biohybrid Systems. Ed. Jung R. Wiley-VCH. 2010. In Press.

Barnett W, Malashchenko T, Cymbalyuk G. Role of slow currents in regulation of bursting activity. Society for Neuroscience meeting, November 2008.

Malashchenko T, Barnett W, Burylko O, Cymbelyuk G. Control of bursting activity by modulation of ionic currents. Eighteenth Annual Computational Neuroscience Meeting: CNS 2009. Berlin, Germany. 18-23 July 2009.

Malashchenko T, Barnett W, Williams D, Cymbalyuk G. Co-existence of bursting and silence of the leech heart interneuron under different pharmacological conditions. Society for Neuroscience meeting, November 2009.

REFERENCES

Ackermans L, Temel Y, Visser-Vandewalle V. Deep brain stimulation in Tourette's Syndrome. Neurothereapeutics. 2008 Apr; 5(2):339-44.

Angstadt JD, Calabrese RL. A hyperpolarization-activated inward current in heart interneurons of the medicinal leech. J Neurosci. 1989 Aug; 9(8):2846-57.

Butera RJ Jr, Wilson CG, Delnegro CA, Smith JC. A methodology for achieving high-speed rates for artificial conductance injection in electrically excitable biological cells. IEEE Trans Biomed Eng. 2001 48: 1460-1470.

Cymbalyuk GS, Calabrese RL. A model of slow plateau-like oscillations based upon the fast Na+ current in a window mode. Neurocomputing. 2001 159: 38-40.

Cymbalyuk GS, Gaudry Q, Masino MA, Calabrese RL. Bursting in leech heart interneurons: cell-autonomous and network-based mechanisms. J Neurosci. 2002 Dec 15;22(24):10580-92.

Dorval AD, Christini DJ, White JA Real-Time linux dynamic clamp: a fast and flexible way to construct virtual ion channels in living cells. Ann Biomed Eng. 2001; 29: 897-907.

Eisen JS, Marder E. A mechanism for production of phase shifts in a pattern generator. J Neurophysiol. 1984 Jun; 51(6): 1375-93.

Fayad JN, Otto SR, Shannon RV, Brackmann DE. Auditory Prostheses "Neural Interface for Hearing Restoration: Cochlear and Brain Stem Implants." 2008 July; 96(7):1085-94.

Friesen WO, Pearce RA. Mechanisms of intersegmental coordination in leech locomotion. Seminars in Neuroscience. Feb 1993; 5(1): 41-47.

Guttman R, Lewis S, Rinzel J. Control of repetitive firing in suid axon membrane as a model for a neuroneoscillation. J Physiol. 1980 Aug; 305:377-95.

Hill AA, Lu J, Masino MA, Olsen OH, Calabrese RL. A model of a segmental oscillator in the leech heartbeat neuronal network. J Comput. Neurosci. 2001; 10:281-302.

Hodgkin A and Huxley A. A quantitative description of membrane current and its application to conductions and excitation in nerve. 1952; 117:1085-94.

Hooper SL. Phase maintenance in the pyloric pattern of the lobster (Panulirus interruptus) stomatogastric ganglion. J Comput Neurosci. 1997 Jul; 4(3): 191-205.

Hooper SL, Buchman E, Weaver AL, Thuma JB, Hobbs KH. Slow conductances could underlie intrinsic phase-maintaining properties of isolated lobster (Panulirus interruptus) pyloric neurons. J Neurosci. 2009 Feb 11; 29(6): 1834-45.

Jung R, Brauer EJ, Abbass JJ. Real-time interaction between a neuromorphic electronic circuit and the spinal cord. IEEE Trans Neural Syst Rehabil Eng. 2001 Sep;9(3):319-26.

Kullmann PH, Wheeler DW, Beacom J, Horn JP. Implementation of a fast 16-Bit dynamic clamp using LabVIEW-RT. J Neurophysiol. 2004 Jan; 91(1):542-54.

Lemasson G, Marder E, Abbott LF. Activity-dependent regulation of conductances in model neurons. Science. 1993 Mar 26;259(5103):1915-7.

Liu Z, Golowasch J, Marder E, Abbott LF. A model neuron with activity-dependent conductances regulated by multiple calcium sensors. J Neurosci. 1998 Apr 1;18(7):2309-20.

LuthiA, McCormick DA. Modulation of a pacemaker current through Ca^{2+} induced stimulation of cAMP production. Nat Neurosci. 1999 Jul; 2(7): 634-41.

LuthiA, McCormick DA. Periodicity of thalamic synchronized oscillations; the role of Ca^{2+} mediated upregulation of I_h. Neuron. 1998 Mar; 20(3); 556-63.

Mahowald M, Douglas R. A silicon neuron. Nature. 1991 Dec 19-26;354(6354:515-8.)

Manor Y, Nadim F. Synaptic depression mediates bistability in neuronal networks with recurrent inhibitory connectivity. J Neurosci. 2001; 21:9460-9470.

Marder E, Prinz AA. Current compensation in neuronal homeostasis. Neuron. 2003 Jan 9;37(1):2-4.

McCormick DA, Pape HC. Noradrenergic and serotonergic modulation of a hyperpolarization-activated cation current in thalamic relay neurons. J Physiol. 1990 Dec; 431: 319-42.

Milescu LS, Yamanishi T, Ptak K, Mogri MZ, Smith JC. Real-time kinetic modeling of voltage-gated ion channels using dynamic clamp. Biophys J. 2008 Jul; 95(1): 66-87.

Moro E, Lang AE. Criteria for deep-brain stimulation in Parkinson's disease: review and analysis. Expert Rev Neurother. 2006 Nov; 6(11):1695-705.

Nadim F, Booth V, Bose A, Manor Y. Short-term synaptic dynamics promote phase maintenance in multi-phasic rhythms. Neurocomputing. 2003 Jun; 52(54): 79-87

Nadim F, Olsen OH, De Schutter E, Calabrese RL. Modeling the leech heartbeat elemental oscillator. I. Interactions of intrinsic and synaptic currents. J Comput Neurosci. 1995; 2:215-235.

Norris BG, Weaver AL, Morris LG, Wenning A, Garcia PA, Calabrese RL. A central pattern generator producing alternative outputs: temporal pattern of premotor activity. J Neurophysiol. 2006 Jul; 96(1): 309-26.

Norris BG, Weaver AL, Wenning A, Garcia PS, Calabrese RL. A central pattern generator producing alternative outputs: phase relations of leech heart motor neurons with respect to premotor synaptic input. J Neurophysiol. 2007 Nov; 98(5): 2983-91.

Olsen OH, Calabrese RL. Activation of intrinsic and synaptic currents in leech heart interneurons by realistic waveforms. J Neurosci 1996; 16: 4958-4970.

Olypher A, Cymbalyuk G, Calabrese RL. Hybrid systems analysis of the control of burst duration by low-voltage-activated calcium current in leech heart interneurons. J Neurophysiol. 2006 Dec; 96(6):2857-67.

Opdyke CA, Calabrese RL. A persistent sodium current contributes to oscillatory activity in heart interneurons of the medicinal leech, J. Comput. Physiol. 1994 Dec; 175(6):781-9.

Ostrem JL, Starr PA. Treatment of dystonia with deep brain stimulation. Neurotherapeutics. 2008 Apr; 5(2):320-30.

Paydafar D, Forger DB, Clay JR. Noisy inputs and the induction of on-off switching behavior in a neuronal pacemaker. J Neurophsyiol. 2006 Dec;96(6):3338-48.

Peck JH, Nakanishi ST, Yaple R, Harris-Warrick RM. Amine modulation of the transient potassium current in identified cells of the lobster stomatogastric ganglion. J Neurophysiol. 2001 Dec; 86(6):2957-65.

Pinto RD, Elson RC, Szucs A, Rabinovich MI, Selverston AI, Abarbanel HD. Extended dynamic clamp: controlling up to four neurons using a single desktop computer and interface. J Neurosci Methods. 2001; 108: 39-48.

Prinz AA, Abbot LF, Marder E. The dynamic clamp comes of age. Trends Neurosci. 2004 Apr;27(4):218-24.

Rachmuth G, Poon CSl. Transistor analogs of emergent iono-neuonal dynamics. HFSP J. 2008 Jun;2(3):156-66.

Schmidt J, Calabrese RL. Evidence that acetylcholine is an inhibitory transmitter of heart interneurons. J Exp Biol. 1992 Oct; 171:329-47.

Sharp AA, O'Neil MB, Abbott LF, Marder E. The dynamic clamp: artificial conductances in biological neurons. Trends Neurosci. 1993; 16: 389-394.

Siegel M, Marder E, Abbot LF. Activity-dependent current distributions in model neurons. Proc Narl Acad Sci USA. 1994 Nov 22;91(24):11308-12.

Shillnikov A, Cymbalyuk G. Transition between tonic spiking and bursting in a neuron model via the blue-sky catastrophe. Phys Rev Lett. 2005 Feb 4;94(4):048101.

Shilnikov AS, Calabrese RL, Cymbalyuk, GS. Mechanism of bistability: Tonic spiking and bursting in a neuron model. Phys Rev E. 2005: 71.

Sorensen M, Deweerth S, Cymbalyuk G, Calabrese RL. Using a hybrid neural system to reveal regulation of neuronal network activity by an intrinsic current. J Neurosci. 2004 Jun 9;24(23):5427-38.

Tass PA, Majtanik M. Long-term anit-kindling effects of desynchronizing brain stimulation: a theoretical study. Biol Cybern. 2006 Jan; 94(1):58-66.

Wallen W, Williams TL. Fictive Locomotion in the lamprey spinal cord in vitro compared with swimming in the intact spinal animal. J Physiol. 1984; 347: 225-239

Wenning A, Hill AA, Calabrese RL. Heartbeat control in leeches. II. Fictive Motor Pattern. J Neurophysiol. 2004 Jan; 91(1):397-409.